# 3-dimensional trapdoor structure of laccolith-induced doming and implications for laccolith emplacement, Pampa Amarilla, Mendoza Province, Argentina

Olivier Galland [a], [*], Hernán de la Cal [b], José Mescua [c], [d], Ole Rabbel [a]

[a] *The NJORD Centre, Department of Geosciences, University of Oslo, Box 1047, Blindern, 0316 Oslo, Norway*
[b] *ROCH S.A., Avenida Madero 1020, Piso 21, Buenos Aires, Argentina*
[c] *Instituto Argentino de Nivología, Glaciología y Ciencias Ambientales, CCT Mendoza, CONICET, Av. Ruiz Leal s/n, Parque Gral. San Martín, Mendoza 5500, Argentina*
[d] *Facultad de Ciencias Exactas y Naturales, Universidad Nacional de Cuyo, Padre Contreras 1300, Parque Gral. San Martín, Mendoza 5500, Argentina*

## ARTICLE INFO

## ABSTRACT

Laccolith emplacement and growth are controlled by doming of overburden rocks. Understanding the mechanics and structural evolution of laccolith-induced doming is therefore essential for revealing the emplacement dynamics and growth of laccoliths. In this paper, we present a 3D reconstruction of a subsurface laccolithic intrusion through the structural reconstruction of a well-exposed dome at Pampa Amarilla, Neuquén Basin, southern Mendoza province, Argentina. The 3D reconstruction was made possible by the unique integration of surface geological data and subsurface 3D seismic and borehole data. We estimate that the Pampa Amarilla laccolith is ~400 m thick, ~3 km and 2.5 km long in the *E*-W and N-S directions, respectively. Along an E-W cross section, the laccolith exhibits a wedge shape with maximum thickness near its western edge and gradual thinning toward the east. The structure of the dome is typical of a trapdoor, with faulting along the western, northwestern and southwestern edges, and tilting of the overburden to the east. The trapdoor tilting of the laccolith's overburden was the main mechanism controlling the thickening and growth of the Pampa Amarilla laccolith, which exhibits a relatively high thickness-to-length ratio $T/D \sim 0.13$. Numerous laccolithic intrusions exhibit similar values of $T/D$, and our study suggests that faulting commonly controls emplacement of laccoliths with $T/D > 0.1$; conversely, our study suggests that the established mechanical models of laccolith emplacement based on elastic bending of the overburden applies only to thin laccoliths. Finally, our study highlights the necessity and value of integrating field geological measurements with subsurface 3D seismic and borehole data for structural reconstructions of subsurface laccolith intrusions.

## 1. Introduction

The dynamics of volcanic plumbing systems control the transport of magma through the crust, and condition whether magma erupts or not at the Earth's surface (Hogan et al., 1998; Burchardt and Galland, 2016; Burchardt, 2018). Sub-vertical magma conduits such as dykes and pipes transport magma upward, whereas sub-horizontal conduits such as sills and laccoliths lead to substantial lateral transport, storage or stalling of magma (Castro et al., 2016; Magee et al., 2016; Galland et al., 2018), which can eventually evolve and form shallow magma reservoirs (Rocchi et al., 2002; Rocchi et al., 2010; Sigmarsson et al., 2011; Castro et al., 2016). The emplacement of sills and laccoliths also trigger significant deformation of the Earth's surface (Minakami et al., 1951;

Donnadieu and Merle, 2001; Kennedy et al., 2012; van Wyk de Vries et al., 2014; Castro et al., 2016; Magee et al., 2017).

The mechanisms controlling magma accumulation and storage in laccoliths depend to a great extent on the deformation mechanism of the overburden (Corry, 1988). One end-member model proposed to explain the emplacement of laccoliths is based on the elastic bending of overlying strata, which are considered as a thin, stiff plate (e.g., Pollard and Johnson, 1973; Koch et al., 1981; Kerr and Pollard, 1998; Bunger and Cruden, 2011; Michaut, 2011; Scheibert et al., 2017). This model end-member is widely implemented as the mathematical formulation of a thin, stiff bending plate is relatively easy to address. This model end-member formulation is valid only for very shallow laccoliths (depth-to-diameter ratio H/D < 0.1) with low thickness-to-diameter aspect ratios

---

[*] Corresponding author.
*E-mail address:* olivier.galland@geo.uio.no (O. Galland).

of the intrusions (T/D < 0.02) (Ventsel and Krauthammer, 2002). However, most laccoliths documented on Earth do not fulfill these geometrical conditions (Corry, 1988; Cruden et al., 2018), as most laccoliths exhibit higher values of H/D, and some intrusions are almost as thick as they are wide (e.g., Minakami et al., 1951; Jackson and Pollard, 1990; Jackson, 1997; Rodriguez Monreal et al., 2009; van Wyk de Vries et al., 2014; Mattsson et al., 2018; Burchardt et al., 2019). In addition, field observations show that significant fracturing and faulting (i.e., inelastic deformation) can accommodate doming of laccolith overburdens (de Saint-Blanquat et al., 2006; Stevenson et al., 2007; Wilson et al., 2016; Mattsson et al., 2018), as accounted for in the end-member "punched laccolith" model where the overburden lifts up like a rigid piston (Gilbert, 1877; Corry, 1988; Schmiedel et al., 2019).

Classical views and mechanical models of sill and laccolith-induced doming, also called forced folding, typically consider symmetrical doming of the overburden (Corry, 1988; Jackson and Pollard, 1990; Bunger and Cruden, 2011; Magee et al., 2017; Scheibert et al., 2017). Nevertheless, geological observations (Witkind, 1973; Román-Berdiel et al., 1995; de Saint-Blanquat et al., 2006; Stevenson et al., 2007) and geodetic measurements (Amelung et al., 2000; Jónsson et al., 2005) suggest that uplift of the intrusion overburdens can be strongly asymmetrical and accommodated by a peripheral fault on one side of the dome, the so-called trapdoor mechanism. However, little constraints are known about the structure of laccolith-induced trapdoor dome.

Reconstructing the structure of both a laccolith and its associated overburden dome is challenging because they occur at scales of several kilometers (Rocchi et al., 2002; Michel et al., 2008; Leuthold et al., 2012; Westerman et al., 2018). Field studies are limited by exposure conditions, where only parts of the intrusion or parts of the dome of the overburden are exposed (Fig. 1; de Saint-Blanquat et al., 2006; Stevenson et al., 2007; Wilson et al., 2016; Mattsson et al., 2018). Recently, seismic data has been used extensively to explore the structure of volcanic plumbing systems, in particular sills and laccoliths and their associated domes, due to its ability to image kilometer-scale subsurface structures at a resolution of some tens of meters (Trude et al., 2003; Hansen and Cartwright, 2006; Jackson et al., 2013; Magee et al., 2013; Schmiedel et al., 2017b; Reynolds et al., 2021). Nevertheless, even though seismic data allows good imaging of sills, thin laccoliths and simple dome structures, it is less effective for imaging thicker laccoliths associated with high amplitude and structurally complex domes (Fig. 1; Rodriguez Monreal et al., 2009; Delpino et al., 2014; Mark et al., 2018).

In this paper, we describe the structure of a laccolith-induced dome by integrating geological field mapping, 3D seismic data and borehole



**Fig. 1.** Sketch illustrating the goal of the manuscript, which is to integrate surface geological data and subsurface data to constrain the shape and extent of an igneous intrusion and its associated dome. The figure also illustrates the challenge of such data integration: (1) surface data are not sufficient to reconstruct the subsurface structure, especially the shape of the intrusion; (2) the potentially complex structure of the forced fold leads to incoherent seismic data.

data. The case study we present is the Pampa Amarilla dome structure, located in the Malargüe fold-and-thrust belt in the northern Neuquén Basin, Argentina. We highlight the added value of integrating field observations with subsurface data, which allowed us to propose a robust reconstruction of the dome and of its underlying laccolith.

## 2. Geological setting of Pampa Amarilla

### 2.1. Geological evolution of the northern Neuquén Basin

The Pampa Amarilla structure is located in the northern Neuquén Basin, southern Mendoza province, ~50 km to the south of the town of Malargüe and 20 km to the east of the village of Bardas Blancas (Fig. 2A). The Neuquén Basin evolved from an extensional basin in the Triassic-Jurassic-Early Cretaceous to a foreland basin in the Late Cretaceous, and comprises a prolific hydrocarbon province with various proven hydrocarbon plays (Vergani et al., 1995; Howell et al., 2005; Veiga et al., 2020), including producing andesitic sills emplaced in organic-rich shales (Spacapan et al., 2020).

The geodynamic evolution of the Neuquén basin occurred in three main phases. Initiation of the basin started in the Triassic-Jurassic as a series of elongated rifts forming isolated depocentres (Vergani et al., 1995; Yagupsky et al., 2008) (Fig. 3). During the early Jurassic, the Rifting phase subsequently transformed into a back-arc basin dominated by regional thermal subsidence (Sag phase; Fig. 3). This led to the deposition of marine sediments of the Mendoza group, which includes organic-rich shales of the Vaca Muerta and Agrio Fms. These formations constitute two of the main source rocks of the basin. The Vaca Muerta and Agrio Fms. are separated in the study area by the carbonaceous Chachao Fm. (Fig. 3). The end of the Sag phase is marked by the deposition of the Rayoso Gr., which includes gypsum of the Huitrín Fm. The Huitrín Fm. is topped by a 5- to 10-m thick limestone of the La Tosca Mb, and claystone and fine-grained sandstone of the Rayoso Fm. (Fig. 3).

In the late Cretaceous, the tectonic regime changed to compression, initiating a foreland basin phase marked by the deposition of the thick continental sandstones and conglomerates of the Neuquén Gr. (Fig. 3). This stage created a series of fold-and-thrust belts including the Malargüe fold-and-thrust belt through reactivation and inversion of the rift-related normal faults as well as older basement faults (Manceda and Figueroa, 1995; Giambiagi et al., 2009; Mescua and Giambiagi, 2012; Mescua et al., 2014; Barrionuevo et al., 2019; Fennell et al., 2020). The study area is located on the gently-dipping western limb of the Malargüe Anticline (Fig. 2B).

During the Foreland basin stage, particularly the northern part of the Neuquén Basin experienced repeated episodes of extensive volcanism and magmatic intrusion of the sedimentary succession (Nullo et al., 2002; Kay et al., 2006). Magmatic activity in the eastern Malargüe fold-and-thrust belt has been separated into two cycles: a late Oligocene to middle Miocene Molle Eruptive Cycle and a middle Miocene to Pliocene Huincán Eruptive Cycle (Fig. 3). The Molle Eruptive Cycle is associated with retroarc volcanism and the Huincán Eruptive Cycle to arc volcanism (Groeber, 1946; Baldauf et al., 1997; Nullo et al., 2002; Combina and Nullo, 2011; Litvak et al., 2015). Both cycles are characterized by predominantly basaltic and andesitic lava flow sequences and subvolcanic bodies such as sills, dykes and laccoliths (Baldauf et al., 1997; Combina and Nullo, 2011; Spacapan et al., 2016, 2017; Spacapan et al., 2020). The youngest volcanism is located toward the east, in the Quaternary Payenia Basaltic Province (Galland et al., 2007; Ramos and Folguera, 2011; Søager et al., 2013).

Magmatism in the Neuquén Basin has substantial economic implications, as it deeply affected local petroleum systems in several ways. First, it provided the necessary heat to generate hydrocarbons from the Vaca Muerta and Agrio Fms., which are mainly immature in the study area (Rodriguez Monreal et al., 2009; Spacapan et al., 2018a; Spacapan
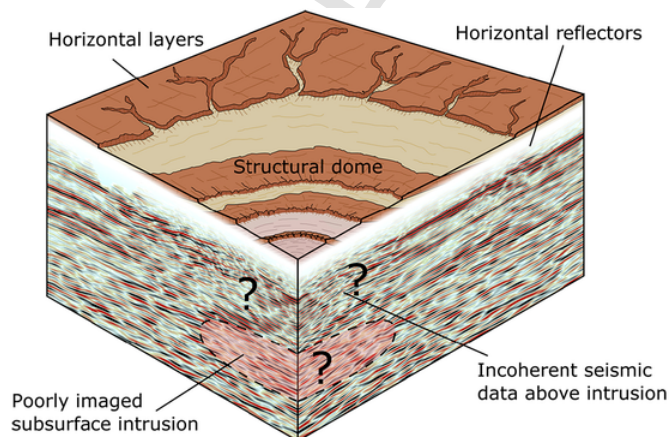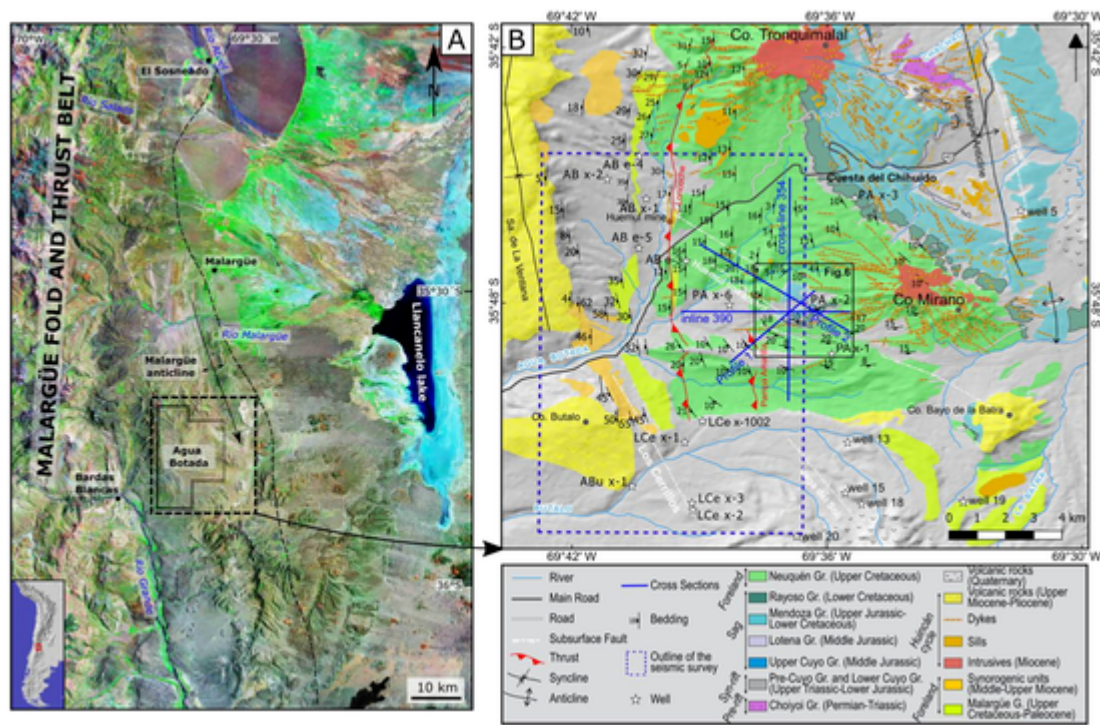
**Fig. 2.** A. Satellite image locating the study area including the Agua Botada block (black solid lines polygon) and surroundings main structures (base image is a LANDSAT7+ satellite image (RGB741 band combination)). Black dashed rectangle locates map of B. Modified from Barrionuevo et al. (2019). B. Main geologic units and structures in the Agua Botada area. Based on YPF (1976). Modified from Barrionuevo et al. (2019). Blue dashed rectangle locates 3D seismic survey used in this study. Black box locates the detailed geological map of Fig. 6. Blue segments locate geological cross sections of Fig. 10. (For interpretation of the references to colour in this figure legend, the reader is referred to the web version of this article.)

et al., 2020). Secondly, the intrusions themselves act as naturally fractured reservoirs, constituting atypical petroleum systems such as the Rio Grande Valley (RGV) oil fields, south of the study area (Schiuma and Llambías, 2014; Rodriguez Monreal et al., 2009; Witte et al., 2012; Spacapan et al., 2020).

### 2.2. The Pampa Amarilla structure

A thick igneous body at Pampa Amarilla, in the Agua Botada area, has been known since 1937 after the drilling of well PA.x-2, which crossed ~100 m of andesite without reaching the bottom of the intrusion. The first clear documentation of an anticline structure at Pampa Amarilla was on a geological map by a geologist commission of YPF (1976) (YPF is the national Argentinian oil company Yacimientos Petrolíferos Fiscales). The map displayed outward-dipping bedding measurements (Fig. 2B), as well as a subcircular outcrop pattern of the Huitrín and Agrio Fms. in the core of the anticline, surrounded by outcrops of red beds of the Neuquén Gr. (Fig. 2B). The geological map of YPF (1976) provided sparse bedding measurements (Fig. 2B), which does not permit the extent, shape and amplitude of the structure to be well constrained.

The map of YPF (1976) highlighted that the Pampa Amarilla structure is located at the boundary between two structural domains: to the north, bedding in the Neuquén Gr. dips gently toward the west, whereas to the south, bedding in the Neuquén Gr. dips gently toward the south (Fig. 2). Probably on this basis, Kraemer et al. (2011) interpreted this structure as a "satellite back-thrust structure developed at the southern plunge of the Malargüe anticline" of tectonic origin. However, the study area is also located along the Bardas Blancas tectonic lineament, which is an inherited structural discontinuity between two Jurassic half-grabens (Manceda and Figueroa, 1993; Yagupsky et al., 2007), and along the NW-trending Huemul lineament, which Barrionuevo et al. (2019) interpret as recording strike-slip movement

during the Miocene. Barrionuevo et al. (2019) proposed that doming of Neuquén basin strata at Pampa Amarilla was the result of the intrusion of the andesite found in well PA.x-2. Our study further demonstrates that the Pampa Amarilla structure is dominantly a laccolith-induced dome, even if we cannot rule out that a minor tectonic component contributed to its development.

In the Agua Botada sector, Cenozoic intrusive rocks correspond to sills, subvolcanic bodies and dykes with predominantly intermediate compositions (Schiuma, 1994). Available K/Ar ages on dykes in the study area yielded early- to middle-Miocene ages (17.3 ± 0.8 and 14.4 ± 0.7 Ma; Valencio et al., 1970). Andesitic and basaltic andesite sills are predominantly emplaced in units with fine-grained sedimentary intervals, particularly in the organic-rich shale of the Vaca Muerta and Agrio Fms. (Schiuma, 1994; Spacapan et al., 2017; Spacapan et al., 2018b; Barrionuevo et al., 2019; Spacapan et al., 2020). Miocene to Quaternary andesitic and basaltic subvertical dykes are abundant in the easternmost Malargüe fold-and-thrust belt, especially those radiating from the Cerro (Mount) Tronquimalal and Cerro Mirano intrusive complexes (Fig. 2B). Away from these intrusive centers, dykes outcropping in the study area exhibit mainly NW-SE and E-W orientations (Bermúdez and Delpino, 1989; Spacapan et al., 2016; Barrionuevo et al., 2019), suggesting that their emplacement was controlled by pre-existing faults and syn-emplacement tectonic stresses, folding and faulting (Spacapan et al., 2016; Barrionuevo et al., 2019).

Note that the Neuquén Basin stratigraphy includes two evaporite formations (Late Jurassic Auquilco Fm. and Lower Cretaceous Huitrín Fm.; Fig. 3). Evaporite sequences are notoriously associated with salt tectonics, including salt diapirs that can trigger doming similar to that observed at Pampa Amarilla (e.g., Alsop et al., 2000). However, we can rule out that salt tectonics is responsible for the Pampa Amarilla dome for the following arguments: the Huitrín Fm. is included in the structure, indicating that if it was a salt diapir, it would be rooted in the Auquilco Fm. However, Pampa Amarilla is located in proximal parts of
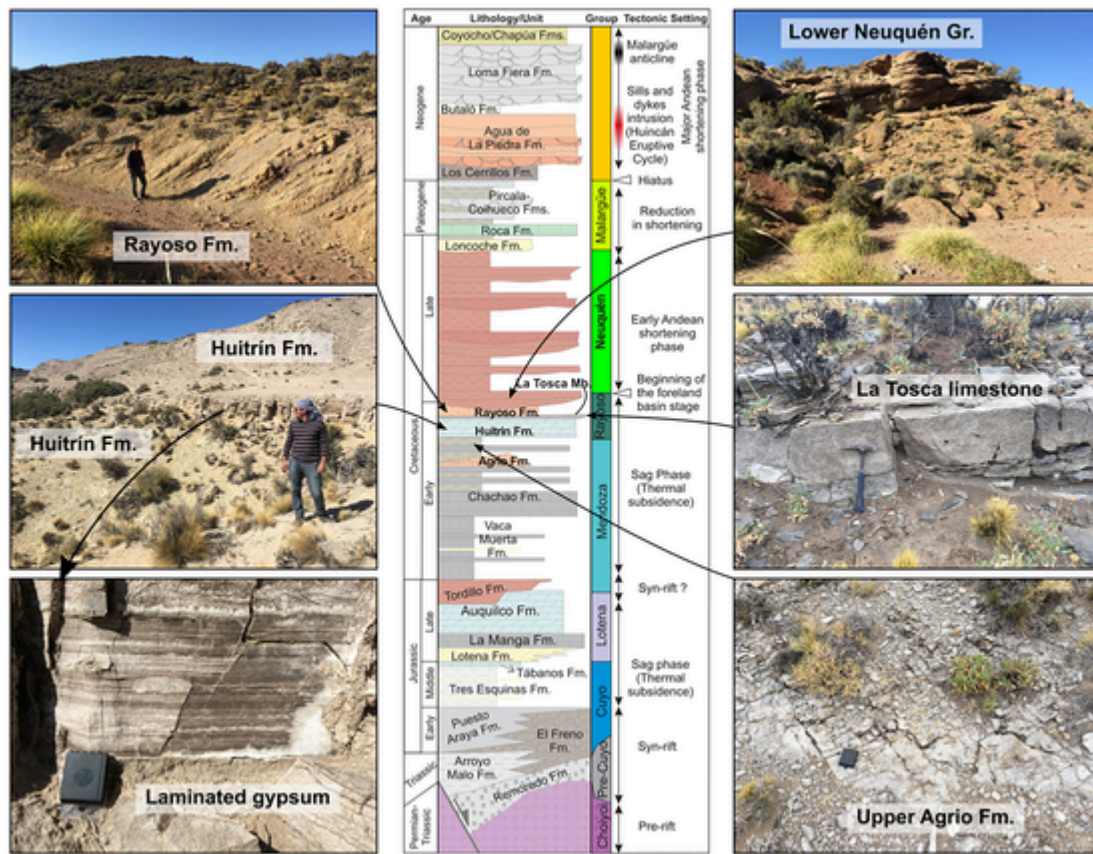
**Fig. 3.** Center. Stratigraphic column showing the sedimentary units, and the main tectonic phases of the Neuquén Basin and Malargüe fold-and-thrust belt (Modified from Giambiagi et al., 2008; Mescua et al., 2014; Horton et al., 2016; Barrionuevo et al., 2019). Left and right. Characteristic field photographs of the outcropping sedimentary units in the study area. Note the unique half a meter thick finely laminated of gypsum within the Huitrín Fm. (lower left photograph).

the Neuquén Basin where the Auquilco Fm. is thin (thickness < 25 m; Fig. 5) and laterally replaced by carbonates.

## 3. Methods and data

### 3.1. Field mapping and drone surveys

We completed detailed field structural mapping of the well exposed Pampa Amarilla structure, which intersects the thin Mesozoic Huitrín and Rayoso Fms. of the Neuquén Basin, in addition to the uppermost Agrio Fm. and the lowermost Neuquén Gr. (Fig. 3). The level of exposure and outcrop quality allowed us to map several stratigraphic contacts almost continuously: Top Agrio Fm./base Huitrín Fm., Huitrín gypsum/La Tosca Mb., Top La Tosca Mb./base Rayoso Fm., and Top Rayoso Fm./base Neuquén Gr. The competent La Tosca Mb. is resistant to erosion, and crops out extensively. We also identified a unique stratigraphic marker within the gypsum of the Huitrín Fm., namely a ~ 50 cm-thick layer of hard, finely laminated gypsum, which separates yellowish (below) and white (above) gypsum deposits (Fig. 3). We collected numerous bedding measurements, notably along the margins of the structure in order to detect sharp bedding changes potentially associated with faulting.

Photogrammetric drone surveys were carried out over the whole Pampa Amarilla structure using a Phantom3 Advanced drone (built-in camera, 12 megapixels). The resulting photographs were processed using Structure-from-Motion photogrammetry software to compute (1) a high-resolution orthorectified image, and (2) a high-resolution Digital Elevation Model (DEM) of the study area (topographic data in Fig. 6). This data was essential for interpretation and lateral interpolation of the field observations.

### 3.2. Seismic and well data

The western half of the Pampa Amarilla dome is covered by a 3D seismic survey associated with hydrocarbon exploration in the Agua Botada block (Fig. 2B). This high-quality seismic data allows a good reconstruction of the subsurface structure north, west and south of the Pampa Amarilla dome (Fig. 4). To the north and to the west, bedding in Mesozoic units dips gently to the west. To the south, Mesozoic units dip gently to the south, as documented in the YPF (1976) map (Fig. 2B). At the location of the Pampa Amarilla dome, the seismic data loses coherency, likely due to imaging difficulties related to the dome structural complexity combined with near-surface high velocity layers (carbonates and evaporites) (Fig. 4). Note that the structure of the Mesozoic units outside the Pampa Amarilla dome is simple with no evidence of faulting. In particular, there is neither seismic nor field evidence of a thrust fault as indicated by YPF (1976) and Barrionuevo et al. (2019) (the proposed Casa de Piedra Thrust).

In addition to the 3D seismic data, geophysical borehole data from two wells have been included in the study (PA.x-2 and PA.x-6; see locations on Fig. 2). Well PA.x-6 displays various geophysical measurements which were used to pick the depth of stratigraphic formation tops with great accuracy (Fig. 5). In addition, this well is within the 3D seismic block, which is convenient to apply a simple vertical geometric scaling of the seismic data (see section 5). We took the data from well PA.x-6 to constrain the thickness and depth of the sedimentary units affected by the Pampa Amarilla dome. We extrapolated the thicknesses of the Mesozoic units measured in well PA.x-6 to the rest of the study area. Given the relatively small extent of the study area, we consider this to be valid first order approximation.
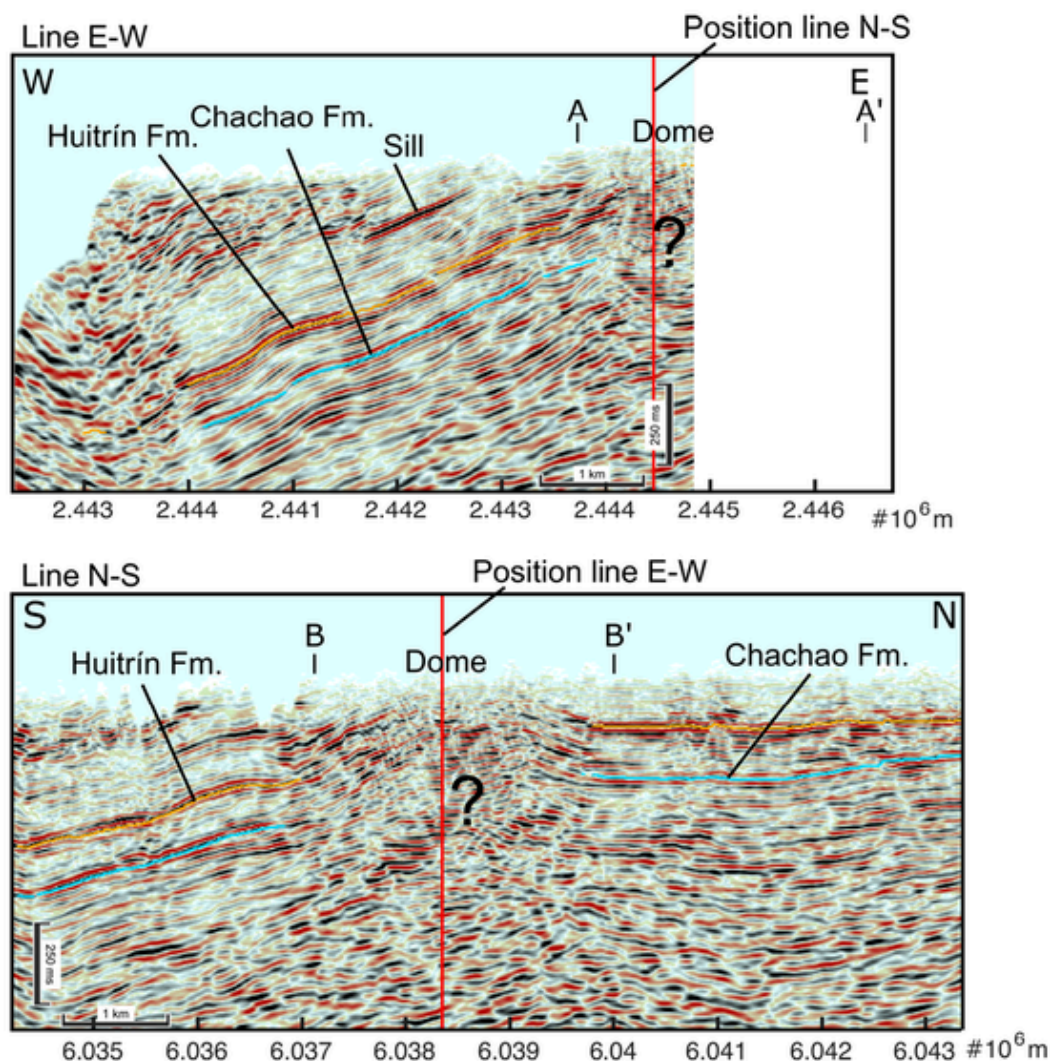
**Fig. 4.** Examples of seismic profiles across the Pampa Amarilla dome (see locations on Fig. 2B) with interpreted tops of the Huitrín (orange lines) and Chachao (light blue lines) formations. A. EW profile showing a gently-dipping monoclinal structure. A forced fold is located on the eastern edge of the profile, where the seismic data is incoherent. B. NS profile showing a gently-dipping monoclinal structure to the south and horizontal layering to the north. A forced fold occurs in the middle of the profile, where the seismic data is incoherent. It is impossible to reconstruct the structure of the dome and the shape and extent of the underlying intrusion on both the EW and NS lines. (For interpretation of the references to colour in this figure legend, the reader is referred to the web version of this article.)

In contrast to well PA.x-6, well PA.x-2 is old (1937–1938), without geophysical log measurements, and the interpretation of the unit thickness and depth was only derived from rock chip cuttings. Even though this well is located in the middle of the dome structure, the uncertainties in the unit depths are too large for it to be useful for reconstruction of the Pampa Amarilla dome. The only data we used from this well is the depth of the roof of the igneous body at 416 m, which is seen as a major transition in the rock chip cuttings data.

## 4. Geological observations

### 4.1. Main stratigraphic contacts

The lithological contrasts between the exposed units at the Pampa Amarilla dome, in addition to the good outcrop quality (Fig. 3), makes mapping of stratigraphic contacts relatively easy. The core of the dome is dissected by an almost E-W trending valley, subsequently referred to as the "Central Valley" (Fig. 6). These exposed stratigraphic units are, from bottom to top, (1) the Agrio Fm. that consists of distal carbonate-rich pelite deposits, (2) the Huitrín Fm. that consists of gypsum deposits topped by limestones of the La Tosca Mb., and (3) the Rayoso Fm. com-

prising light brown clay to very fine-grained sand deposits (Fig. 3). These units are covered by coarse red sandstone and conglomerate of the Neuquén Gr.

Stratigraphic contacts between these units are easily mapped along the northwestern, northern, and eastern edges of the dome, but are covered by Quaternary deposits on the southeastern edge of the dome (Fig. 6). The main stratigraphic marker in the study area is the thin carbonate of the La Tosca Mb., which controls the most prominent topographic features of the dome. From there, we mapped the Top La Tosca Mb./ base Rayoso Fm. contact in detail. The fine-grained Rayoso Fm. outcrops poorly, but the transition between the top Rayoso Fm./base Neuquén Gr. is well marked by a dark grey conglomerate bed, which can be followed in the landscape.

### 4.2. Mapping of bedding

We collected a high density of bedding plane measurements, especially where bedding orientation is observed to change sharply (Fig. 6). Such measurements are not equally straightforward in all the units exposed in the area, where sandstone to conglomerate beds of the
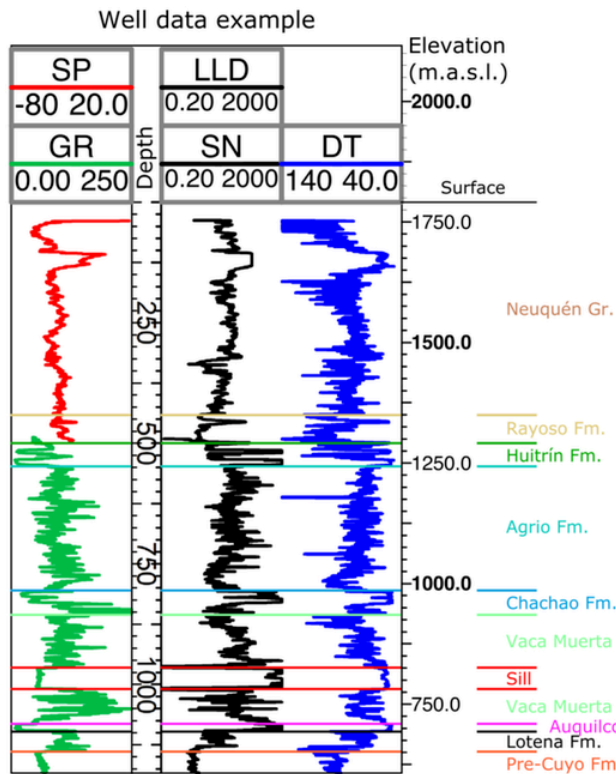
## Well data example



**Fig. 5.** Geophysical borehole data from well PA.x-6 (see location on Fig. 2B). SP: spontaneous potential (millivolts); GR: Gamma Ray (API units); LLD/SN: resistivity (Ohms); DT: transit time (microseconds per foot). Formation tops can be identified from sharp variations of geophysical borehole data.

Neuquén Gr. are highly irregular and very few well-defined beds are exposed in the Rayoso Fm.

Due to the scale of the mapping the structure above the intrusion was characterized in greater detail than previous studies, documenting sharp variations in bedding orientation. Steeply-dipping bedding planes were measured along the western edge of the dome (up to 70°; Fig. 7E), in good agreement with the narrow outcrop width of the Rayoso Fm. (Fig. 6). Along the western edge of the dome, bedding transitions from steeply to gently-dipping (<15°) over a distance of 200–300 m only. Sub-vertical layers of the Agrio Fm. (84°) are observed close to the center of the dome, a few tens of meters from the gently-dipping La Tosca Mb. in the southern limb of the dome (Fig. 6). In contrast, bedding in the eastern limb dip very gently, in agreement with large outcrop width of the La Tosca Mb and Rayoso Fm. (Fig. 6). The bedding measurements indicate that the Pampa Amarilla dome is strongly asymmetric.

The carbonate layers of the La Tosca Mb. exhibit numerous short wavelength (<10 m) folds. We inferred that these structures could not be related to larger-scale deformation, but instead related to folding due to the detachment of the beds of La Tosca Mb. with respect to the underlying gypsum of the Huitrín Fm.

### 4.3. Deformational structures

A number of deformational structures in the Mesozoic sedimentary formations are associated with the Pampa Amarilla dome structure. These structures provide insights on the shape and deformational style of the dome.

*Faults.* An *E*-W striking, steeply northward-dipping normal fault with an offset of several meters is observed continuously along the northern scarp of the Central Valley (Fig. 7B). We interpreted several other faults based on breaks in stratigraphy and sharp variations in bedding dips (Figs. 6 and 7).

*Folds.* Folds can be observed at different scales. At relatively large scale (>100 m), on the western edge of the dome, an eastward increase in dip from ~10° to ~60° indicates substantial dome-parallel bending of the strata of the Agrio to Rayoso Fm. Dome-parallel, ENE-WSW trending meter-scale folds occur in the Rayoso Fm. (Fig. 7F,G).

*Ductile foliation.* A ductile foliation is observed in the gypsum of the Huitrín Fm. (Fig. 7D). Such ductile deformation was only observed along the western edge of the dome, i.e. where the bedding is the steepest (Fig. 6). The foliation planes contain a down-dip lineation indicating E-W stretching perpendicular to the edge of the dome at this locality. Because of the very local expression of this ductile deformation, we interpret these structures as a result of shearing along the gypsum during dome growth.

### 4.4. Igneous intrusions

A number of E-W trending, variably exposed, fine-grained andesitic dykes are observed traversing the dome (Fig. 6) (Barrionuevo et al., 2019). A few sills are also observed in the Mesozoic sedimentary units. The most prominent sill is located at the eastern edge of the dome (Fig. 6). It is made of a very coarse-grained andesite, with several centimeters size amphibole phenocrysts. It was emplaced at the contact between the top La Tosca Mb. and the base Rayoso Fm., clearly controlled by the lithological contrast between these two formations. Its thickness is challenging to estimate, because the sill and the La Tosca/Rayoso stratigraphic contacts are almost parallel to the topography. The distinct phenocrysts sizes in the dykes and the sill show that the magmas were injected during distinct pulses of magmas of distinct differentiation histories.

### 4.5. Summary of geological observations

The main conclusions from our geological observations are the following:

- Deformation of the Mesozoic units is restricted to the vicinity of the dome. From this we conclude that the Pampa Amarilla dome is a local structure associated with an underlying igneous intrusion, and not a tectonic structure;
- The dome has an asymmetric structure, with a steeply-dipping western edge and a shallow-dipping eastern edge;
- Several faults dissect the center of the dome. There may be many more faults in the central part that are not exposed.

These geological observations are not sufficient to constrain the shape, extent and thickness of the underlying intrusion responsible for the formation of the Pampa Amarilla dome. The geological data are integrated with 3D seismic and well data below to construct structural cross sections.

## 5. Structural cross sections

We constructed four cross sections across the Pampa Amarilla dome. The E-W and N-S oriented cross sections follow the in-line 390 and cross-line 354 seismic profiles, respectively. The SW-NE Profile1 and NW-SE Profile2 were chosen to intersect the approximate center of the dome. Note that the E-W L390 profile is located 100 to 200 m south of wells PA.x-2 and PA.x-6. We chose this location to incorporate the faults and observed stratigraphic contacts south of the Quaternary cover of the Central Valley (Fig. 6). Note that the structure at the location of well PA.x-6 is simple, with gently dipping strata to the west (Figs. 2B and 4). Therefore, the depths of the formation tops in well PA.x-6 can be confidently extrapolated to the location of E-W cross section L390.
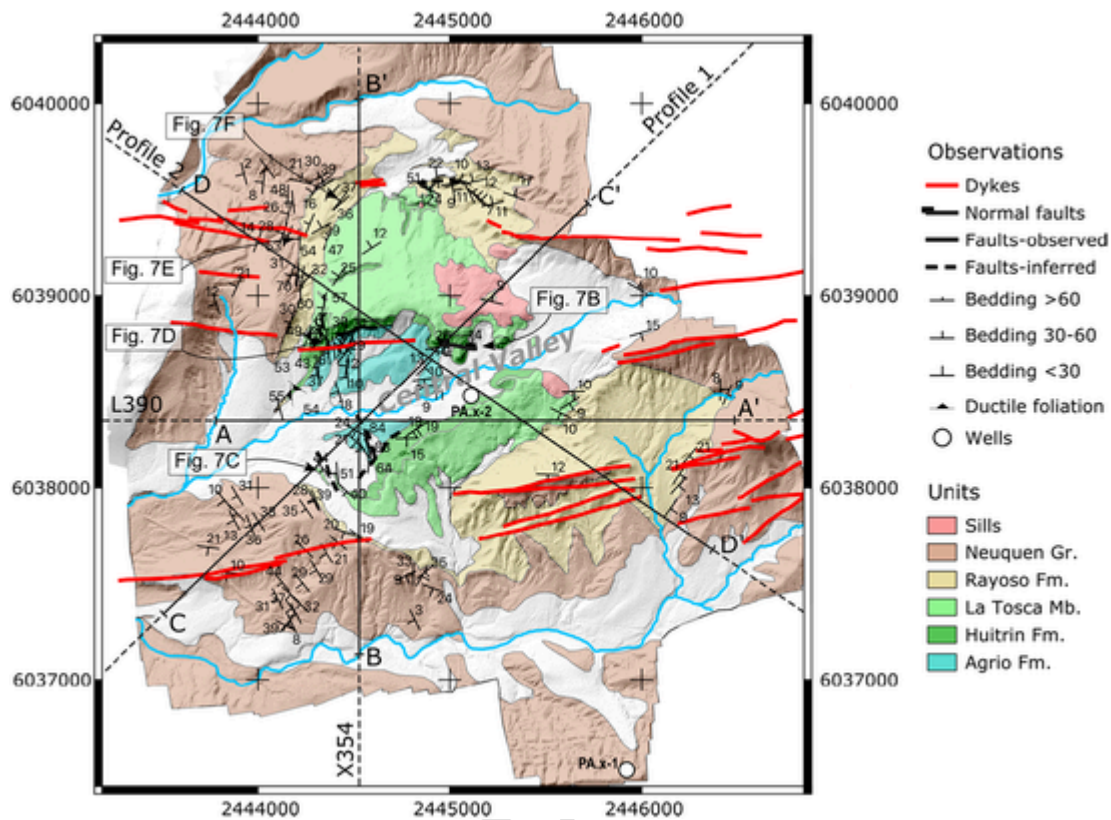
**Fig. 6.** Geological map of the Pampa Amarilla dome (see location in Fig. 2) showing structural field measurements, locations of structural observations (Fig. 7), seismic profiles (Fig. 4) and geological cross sections (Fig. 10). Topography data were calculated from photogrammetric drone surveys. The coordinate system of the map is the Campo Inchauspe / Argentina 2 EPSG:22192.

### 5.1. Vertical scaling of seismic data

Since the seismic data are only available in two-way travel time, we performed a time-to-depth conversion in order to be able to integrate it with the field data. Note that where abundant borehole and check-shot survey data are available, this conversion is typically performed using advanced seismic interpretation software. However, because only one modern well is available, we carried out a manual vertical scaling, using the following steps (summarized in Fig. 8):

- A high-resolution topographic map of the area was computed from the photogrammetric drone survey images.
- Topographic profiles were constructed along the seismic profiles going through well PA.x-6, and the depth of the top Huitrín Fm. in the well was integrated with the topographic data (Fig. 8, upper left).
- In a seismic interpretation program, the topographic map was converted into time to be integrated with the 3D seismic cube. Thus, topographic profiles can be incorporated into seismic profiles (Fig. 8, lower left).
- The prominent top Huitrín Fm. reflector was interpreted on the selected seismic profiles (orange line Fig. 8, lower left).
- The vertical scales of these seismic profiles were linearly transformed such that both (1) the time-converted topography matched the true topography and (2) the position of the top Huitrín Fm. reflector matched the depth of top Huitrín Fm. in the well (Fig. 8, right);
- We used the seismic profile at the location of the well to adjust the vertical scale of the other profiles used to construct the four cross sections.

Given that the various lithologies of the local stratigraphy have distinct geophysical properties, this linear transformation of the vertical scale of the seismic data is a crude approximation of reality. However, the structure to the west of the dome is a simple monocline and the calculated dip angle of the reflectors match the bedding surface measurements very well (~15°; Figs. 2B and 8). Furthermore, the aim of this rescaling of the seismic data is not to calculate the depth of all units, but to constrain the structure (i.e. the dip angle) of the main stratigraphic contacts.

### 5.2. Construction of the structural cross sections

Construction of the structural cross sections followed 5 main steps, which are illustrated with cross section L390 (Fig. 9).

Step 1. Vertical scaling of the seismic profile, following the method described in Section 5.1 and Fig. 8 (Fig. 9A).

Step 2. On the topographic profile of the cross section, we placed the mapped stratigraphic contacts and the bedding measurements. In addition, the locations of the faults crossed by the section are also marked (F on Fig. 9B).

Step 3. Using a vertical stratigraphic column defined by the thickness of the units logged in well PA.x-6 (see Fig. 5), and assuming that the unit thicknesses remain constant across the study area, we extrapolate the depth of the unit contacts along the cross sections (Fig. 9C). The same procedure was applied to the Top Huitrín Fm. seismic reflector outside the Pampa Amarilla dome (Fig. 9C).

Step 4. We laterally interpolated the geological horizons to reconstruct part of the structure (Fig. 9D).

Step 5. The geometry of the dome and the underlying intrusion are interpreted at the final step. This step is the most interpretative. First, well PA.x-2 data indicates that the roof of the Pampa Amarilla igneous body is located near the bottom contact of the Vaca Muerta Fm. In the
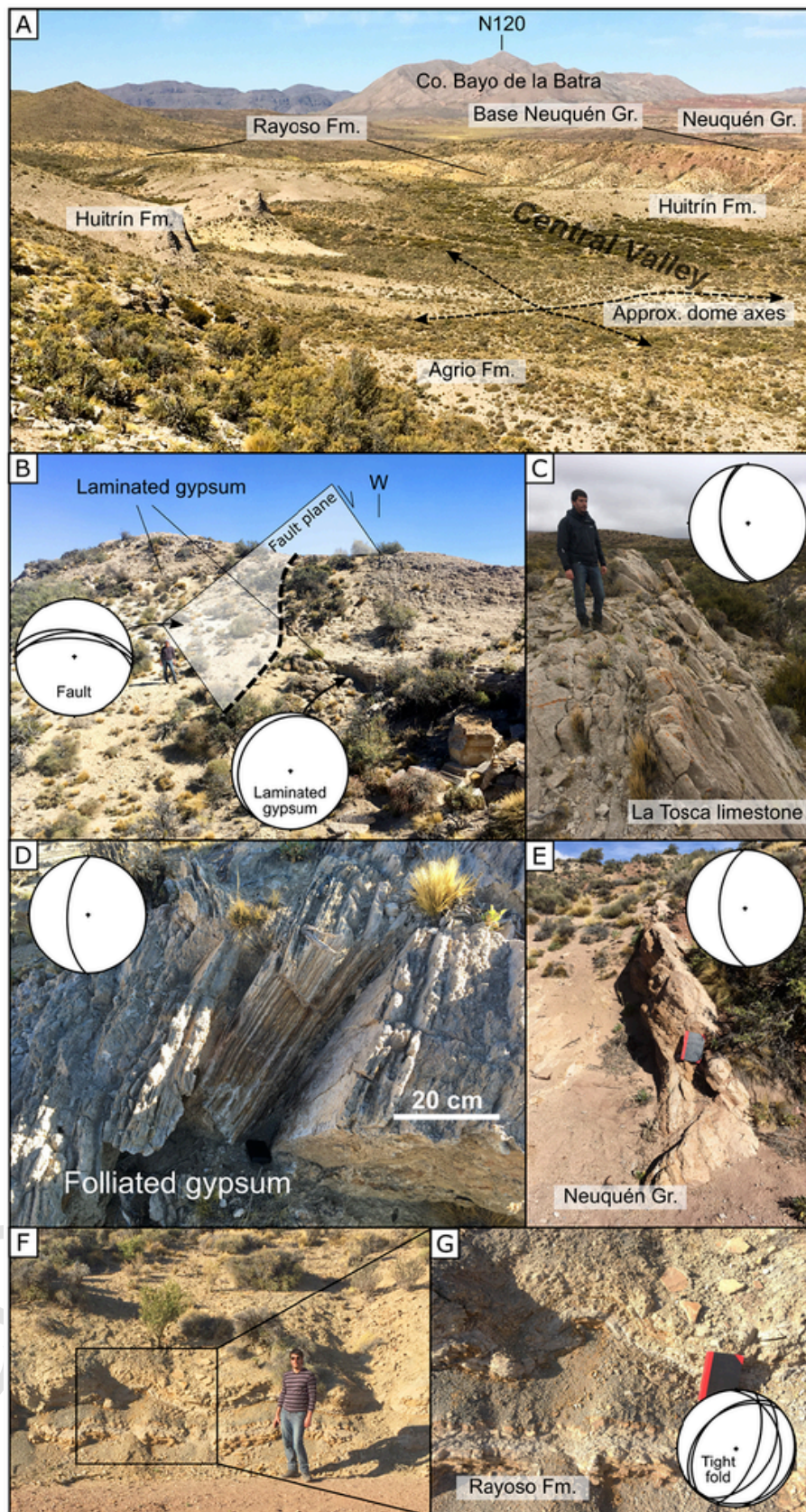
**Fig. 7.** A. Overview field photograph of the Central Valley, in the middle of the Pampa Amarilla dome. View toward SE. B. Photograph of normal fault affecting Huitrín Fm., northern edge of Central Valley (see location on Fig. 6). C. Photograph of steeply dipping limestone of La Tosca Mb., western edge of the dome (see location on Fig. 6). D. Detailed photograph of ductile foliation within gypsum of Huitrín Fm., western edge of the dome (see location on Fig. 6). E. Photograph of

◀ steeply dipping sandstone bank of Neuquén Gr., northwestern edge of the dome (see location on Fig. 6). F. Tight folds in the Rayoso F., northwestern edge of the dome (see location on Fig. 6).
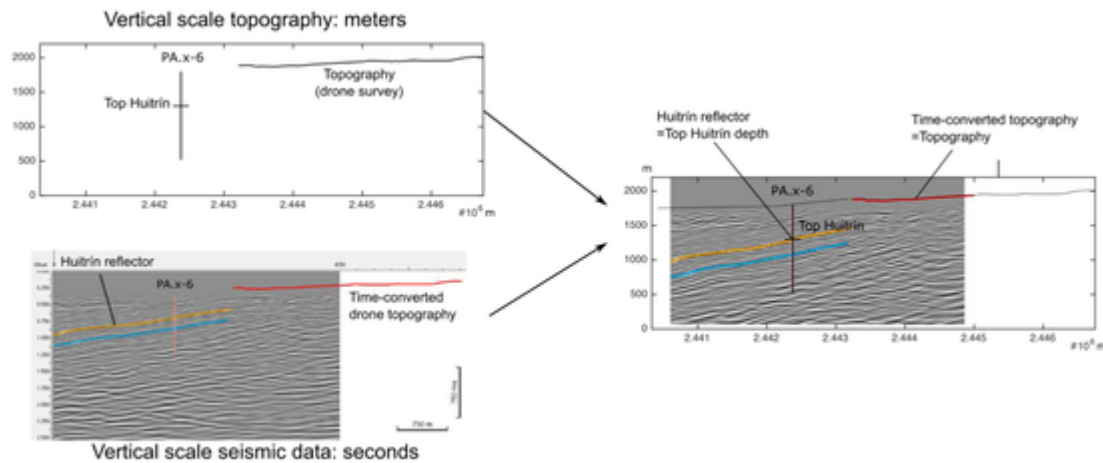


**Fig. 8.** Drawing illustrating the qualitative method implemented to integrate field and borehole (in meters) and seismic (in seconds) data. Top left: topographic profile calculated from drone surveys, with location of well PA.x-6 and identified depth of top Huitrín Fm. (see Fig. 5). Units in meters. Bottom left: seismic profile passing through well PA.x-6, with interpreted tops of the Huitrín Fm. (orange) and the Chachao Fm. (light blue). The red line is topography calculated from the drone survey, converted into time. Units in seconds. Right: vertical scale of seismic profile is adjusted such that the top Huitrín and topography match in both meter-scale and second-scale. (For interpretation of the references to colour in this figure legend, the reader is referred to the web version of this article.)

cross section displayed in Fig. 9D, it is clear that the entire stratigraphic succession in the dome is significantly uplifted with respect to the succession west of the dome, but the base of the intrusion is not resolved. We filled this interpretation gap by correlating this cross section with the other cross sections, especially the N-S trending X354 cross section, on which the top Huitrín Fm. reflector is well resolved on the northern and southern sides of the dome (Fig. 5B). Along profile X354, we applied Step 1 to Step 4 of the procedure described above, and we interpolated the base Vaca Muerta Fm. between both sides of the dome, assuming that the base of the intrusion coincides with the base Vaca Muerta Fm. The depth of the intrusion's base contact on cross section X354, at the crossing point between cross sections L390 and X354, defines a marker point for the basal contact of the intrusion on cross section L390.

### 5.3. Cross sections

Fig. 2 shows the locations of the cross sections presented in Fig. 10.

**Cross section cross-line 354**. This cross section N-S oriented crosses the dome near its centre. There is no significant depth difference of the Vaca Muerta, Chachao and Agrio Formations between the northern and the southern domains of the dome. Although there is a gentle dip difference between the southern and northern parts of the dome, it is not possible to identify a vertical offset. This strongly suggests that the deformation observed in the study area is only related to the emplacement of the laccolith.

When compared to the known thickness of the Agrio to Vaca Muerta Fms., the depth of the roof of the intrusion drilled in well Pa.x-2 suggests that the laccolith was emplaced close to the bottom of the Vaca Muerta Fm. By interpolating the bottom of the Vaca Muerta Fm. from north to south, it is possible to estimate the amplitude of the dome, which is considered to be a good proxy for the thickness of the laccolith, close to 400 m. This allows the depth of the bottom of the intrusion to be estimated, which is consistent with the interpolated base of the Vaca Muerta Fm. across the dome.

The seismic data and the geological map indicate a ~ 400 m depth difference of the top Huitrín Fm., which suggests that the northern edge of the dome is faulted. This interpretation is supported by the local folding and faulting observed in the Rayoso Fm. (Fig. 7F,G).

The exact structure of the southern edge of the dome is unclear. No evidence of faulting is observed at the surface. The structure of this part of the dome is the least constrained of the study area. Nevertheless, the ~400 m depth difference between the top Huitrín Fm. mapped in the field and that identified in the subsurface data indicate significant differential uplift over a small distance, implying that the overlaying strata experienced significant shear strain, likely accommodated by faulting. This indirect evidence of deformation makes the distribution of deformational structures quite speculative due to the lack of exposed structures.

The observed deformation and the cross sections suggest that the N-S dimension of the laccolith is ~2 km.

**Cross section in-line 390**. The structure of the dome along this E-W cross section is asymmetric, with a strongly deformed western edge and a gently-dipping eastern edge (Fig. 10). The significant deformation and the sharp depth difference of the Mesozoic units at the western edge of the dome strongly suggests that it is faulted along one major fault or several smaller faults.

The Mesozoic units at the eastern edge of the dome are structurally higher than to the west of the dome (Fig. 10), suggesting that the laccolith extends beyond the mapped area to the east. The asymmetric deformation of the dome strongly suggests that the uplift was accommodated by a trapdoor mechanism: most of the uplift was accommodated by the fault at the western edge, while the overburden to the east was rotated upward and only gently deformed.

The cross section suggests that the E-W dimension of the laccolith is at least 3 km. Compared to the N-S profile along cross-line 354, we infer that the laccolith is elliptical in shape on map view, with a 3 km long axis trending E-W and a 2 km short axis trending N-S.

**Profile1 and Profile 2**. These profiles confirm the interpretations of cross sections L390 and X354. The faults observed in the field suggest that the trapdoor structure at the western and southwestern edges of the dome has been accommodated by several faults.

## 6. Interpretation

### 6.1. Laccolith shape and deformation style of overburden

The main assumption for reconstructing the shape of the subsurface Pampa Amarilla laccolith is that there was no significant compaction of
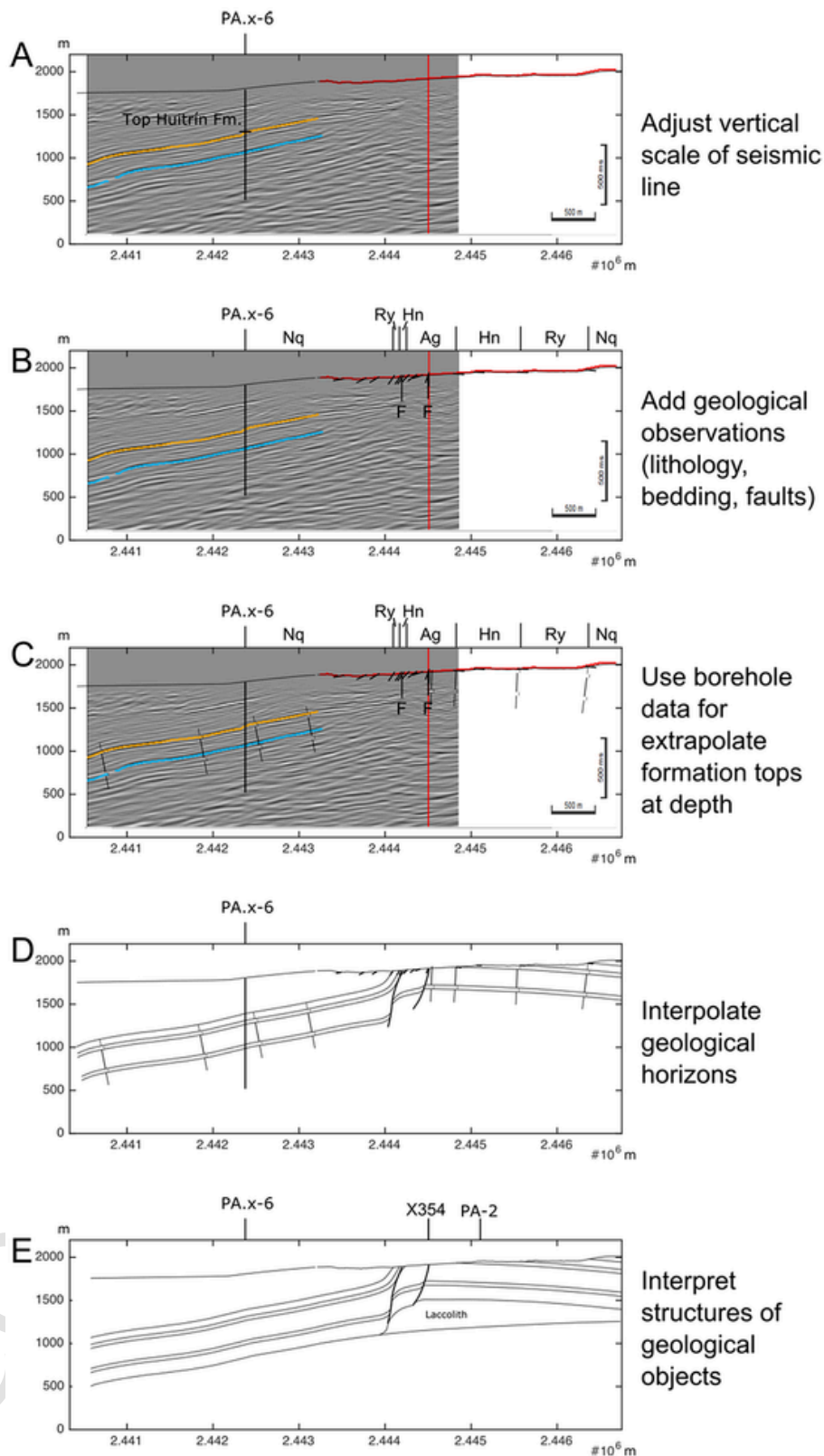
Fig. 9. Schematic drawing illustrating the main steps for constructing the structural cross sections.

the overburden associated with the emplacement. This assumption is supported by the fact that the emplacement depth of the laccolith was between 3000 m and 4000 m at the time of emplacement, i.e. before folding and uplift of the Malargüe anticline (Barrionuevo et al., 2019). At these depths, the host rock formations would have been already compacted. However, we cannot rule out some minor *syn*-emplacement and post-emplacement compaction, which might affect the reconstruction of the Pampa Amarilla dome and underlying laccolith.

The shape of the Pampa Amarilla laccolith is inferred to be asymmetrical, with a maximum $T \sim 400$ m thickness in its western part, and
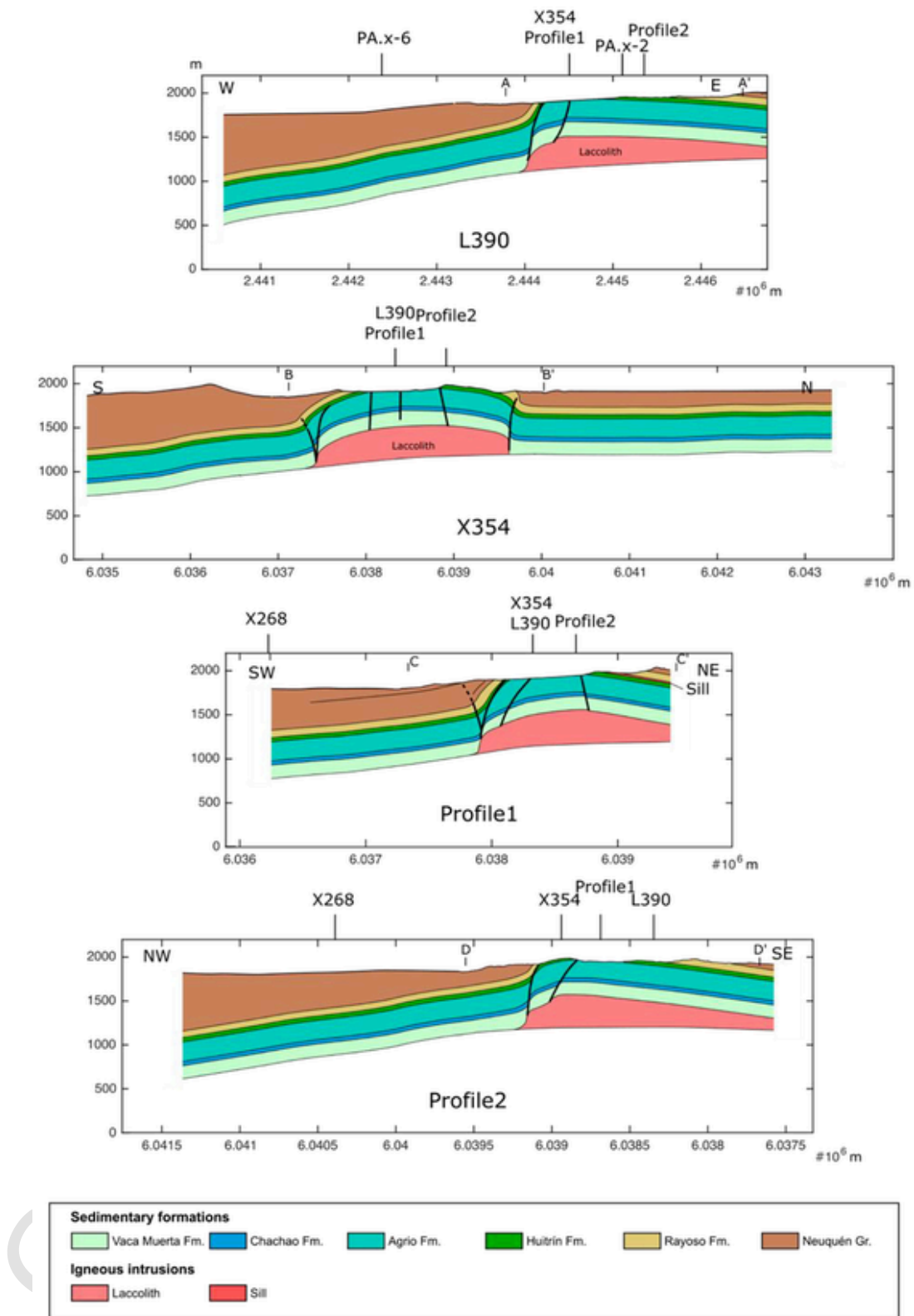
**Fig. 10.** Cross sections. Cross sections are located on Fig. 2B. Segments of the cross sections A-A'. B-B′, C-C′ and D-D′ are located on geological map of Fig. 6. The locations of wells PA.x-2 and PA.x-6 are indicated on Profile L390. The locations of the intersections with other cross sections are indicated on each profile.

thinning toward the east with a wedge shape (Figs. 10 and 11). With a minimum E-W length of $D \sim 3$ km, the laccolith exhibits a thickness-to-length ratio $T/D \sim 0.13$, which is in the typical range for felsic laccoliths (Fig. 12) (Corry, 1988; Cruden et al., 2018). This aspect ratio is one to two orders of magnitude higher than most sheet intrusions, such as

dykes and mafic sills, the typical values of $T/D$ ranging between $10^{-2}$ and $10^{-4}$ (Fig. 12) (Rubin, 1995; Bunger and Cruden, 2011; Cruden et al., 2018). This value of $T/D \sim 0.13$ indicates that the Pampa Amarilla laccolith is much fatter (i.e., higher thickness-to-diameter aspect ratio)
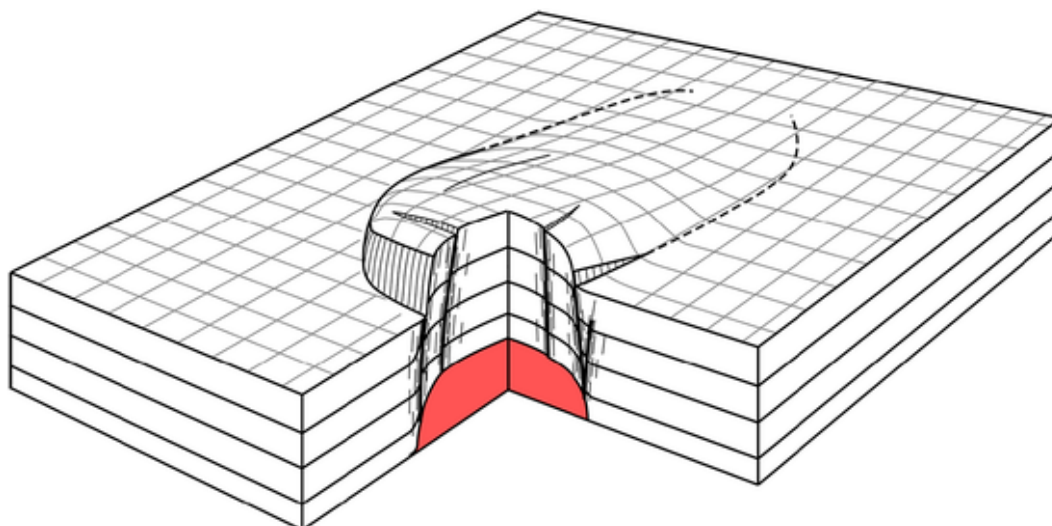
**Fig. 11.** Sketch summarizing the structure of the Pampa Amarilla laccolith and trapdoor dome.
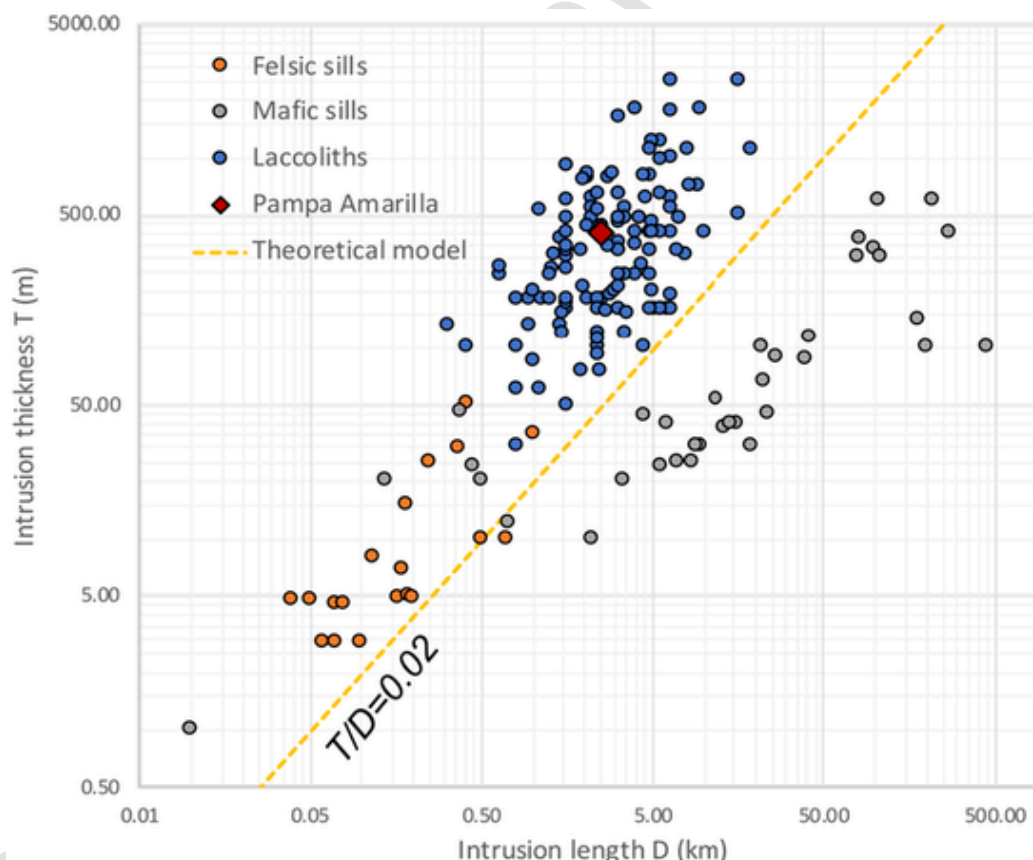


**Fig. 12.** Plot of thickness (in meters) of laccoliths (blue circles), felsic sills (orange circles) and mafic sills (blue circles) and the Pampa Amarilla laccolith (red diamond) as a function of their length (in kilometers). Data from Cruden et al. (2018). (For interpretation of the references to colour in this figure legend, the reader is referred to the web version of this article.)

than sheet-shaped sills, and suggests that its emplacement results from a different mechanism than that of sills.

This value of $T/D$ is compatible with the observed intense deformation of the overburden, given that 400 m of uplift must be accommodated over <3 km. The overall structure of the dome is typical of a trapdoor, with a clear peripheral fault cross cutting its western, northwestern and southwestern edges (Figs. 10 and 11). The very minor deformation observed in the central part of the dome strongly suggests

that it was tilted to the east as a result of differential thickening of the underlying laccolith.

The main boundary fault of the dome is visible at its western edge. However, it is likely that the northern and southern edges of the domes are partly faulted, even if faults are not exposed at the surface. We can estimate whether a fault can be expected by defining the local vertical shear strain $\gamma_v = \Delta h / \Delta x$ along the edges of the dome, where $\Delta h$ is the uplift difference and $\Delta x$ is the distance over which $\Delta h$ is accommodated. On the N-S striking section (Fig. 10), the differential uplift at the

northern edge of the dome is estimated to be $\Delta h \sim 200$ m, accommodated over a short distance $\Delta x < 200$ m (Fig. 10), leading to an estimate of $\gamma_v \sim 100\%$. Such shear strain value cannot be accommodated by elastic bending, and faulting is expected, as evidenced by the tight folds observed in the Rayoso Fm. at the expected fault location (Fig. 7F,G). The southern edge of the dome on the N-S striking section is less pronounced than the northern edge, with a differential uplift $\Delta h \sim 300$ m accommodated over a distance $\Delta x \sim 700$ m, leading to estimate of $\gamma_v \sim 50\%$. Although this local shear strain value is lower than that estimated at the northern boundary, it is much higher than critical strain required for rock failure ($< 1\%$; e.g., Jaeger et al., 2009; Renard et al., 2019). We thus expect faulting, or distributed damage, to affect the southern edge of the dome. Nevertheless, our geological observations and subsurface data are not sufficient to constrain the shape of the southern boundary fault.

Both the N-S and E-W cross sections provide very different pictures of the structure of the laccolith and associated dome (Fig. 10): the E-W cross section highlights a very asymmetrical trapdoor structure, whereas the N-S cross section displays a more symmetrical structure with both edges likely faulted. Such a difference reflects the complex 3-dimensional geometry of both the laccolith and the associated dome, which cannot be captured by a single cross section.

Gypsum within the Huitrín Fm. exhibits prominent ductile deformation along the western edge of the dome, i.e. where it is the most deformed. The foliation within the gypsum is parallel to the strata tilted by the doming, consistent with shearing associated with differential uplift of the dome with respect to the surrounding strata. There is no tectonic structure that can be linked with such foliation in the study area (Fig. 2)(Barrionuevo et al., 2019). We therefore interpret this ductile foliation to be a result of dome growth during the emplacement of the laccolith. This suggests that the gypsum of the Huitrín Fm. may have acted as a local detachment that decoupled the Agrio Fm. from the overlaying Rayoso Fm. and Neuquén Gr., which may have in turn affected the growth of the dome. This interpretation is supported by tectonic studies in the Neuquén Basin, which have recognized that the detachment potential of the Huitrín Fm. deeply affected the style of tectonic deformation (e.g., Cobbold and Rossello, 2003). Therefore, our field observations show that ductile deformation can occur at time scales of magma emplacement, as discussed in Section 6.2.

### 6.2. Laccolith ellipticity and feeder dyke

The orientation of the long axis of the reconstructed Pampa Amarilla laccolith is similar to the orientation of most dykes observed in the study area (Figs. 2 and 6) (Barrionuevo et al., 2019), suggesting that the feeder of the laccolith was an E-W-striking dyke. Such a relationship between the long axis of elliptical tabular intrusions and their feeder dykes has been documented for mafic sills (Galerne et al., 2011; Magee et al., 2016). However, we acknowledge that other processes like magma cooling during emplacement (Currier and Marsh, 2015) can also affect the ellipticity of laccoliths.

The orientation of a potential E-W-striking feeder dyke is compatible with the regional compressional stresses associated with Andean tectonics. To estimate the time-scale of emplacement of the Pampa Amarilla laccolith, we assume that the laccolith was fed by a $L = 3$-km long (the length of the Pampa Amarilla laccolith) and $t = 3$-m thick dyke, which is a characteristic dyke thickness in the study area (Barrionuevo et al., 2019). Typical values of andesitic magma velocities are $v = 0.01$ to 0.1 m s$^{-1}$, thus the volumetric flow rate provided by the feeder dyke would be $Q = L \times t \times v$ between 90 and 900 m$^3$ s$^{-1}$. We estimate the laccolith volume from $V = \pi R^2 T$, where $T = 300$ m is an average value for the laccolith thickness, yielding $V \sim 2.1 \times 10^9$ m$^3$. The time scale of emplacement $T = V/Q$ thus yields a time-scale between $\sim 1$ year and $\sim 1$ month, assuming it formed during one magma pulse. Such results are in good agreement with observations of laccolith

emplacement at active volcanoes (Minakami et al., 1951; Castro et al., 2016). Even if this analysis is simplistic, it shows that the ductile deformation observed in the gypsum of the Huitrín Fm. occurred at time scales orders of magnitude shorter than tectonic deformation time scales.

## 7. Discussion

### 7.1. Magma emplacement mechanics

The trapdoor structure of the Pampa Amarilla dome highlights that the growth of the laccolith is dominantly controlled by faulting and tilting of the overburden. This structure is in good agreement with observations of trapdoor emplacement of laccoliths, such as the Barker Quadrangle laccoliths, Montana (Witkind, 1973; Román-Berdiel et al., 1995), the Black Mesa laccolith, Henry Mountains, Utah (de Saint-Blanquat et al., 2006), the Eastern Mourne pluton, Northern Ireland (Stevenson et al., 2007), or the Sandfell laccolith, eastern Iceland (Hawkes and Hawkes, 1933; Mattsson et al., 2018). These observations are also in agreement with the models of laccolith and sill emplacement based on the Coulomb failure of the overburden (Román-Berdiel et al., 1995; Haug et al., 2017; Schmiedel et al., 2017a; Haug et al., 2018; Schmiedel et al., 2019). These models assume that shear failure of the overburden occurs when the intrusion reaches a critical diameter that depends on (1) the depth of the intrusion, (2) the strength and friction angle of the overburden, and (3) the viscosity and volumetric flow rate of the magma. Once the overburden fails, the intrusion can either thicken by pushing the overburden upward along ring faults if the magma is highly viscous, forming a punched laccolith, or propagate along the planes of weakness of the faults if the magma is of low viscosity to form saucer-shaped intrusions (Schmiedel et al., 2019). At the Pampa Amarilla laccolith, we expect the magma to have been highly viscous, favouring a punched laccolith.

The geometric characteristics of the Pampa Amarilla laccolith are in disagreement with the end member mechanical model of laccolith emplacement based on elastic bending of the overburden (Murdoch, 2002; Bunger and Cruden, 2011; Michaut, 2011; Thorey and Michaut, 2014), which builds on the seminal papers of Johnson and Pollard (1973) and Pollard and Johnson (1973). The main assumptions of these models are the following: (1) the overburden of the intrusion bends elastically as a response of magma overpressure in the intrusion; (2) the basement of the intrusion is rigid. The overburden can be either rigidly attached to the basement (Pollard and Johnson, 1973; Bunger and Cruden, 2011) or attached to the basement through a deformable elastic layer (Kerr and Pollard, 1998; Galland and Scheibert, 2013; Scheibert et al., 2017). In these models, the mathematical formulation of the bending overburden is based on the thin, stiff elastic plate approximation. This model formulation is derived assuming the two following conditions: (1) the thickness of the deforming plate is small with respect to its length, and (2) the deflection of the bending plate is small with respect to the plate thickness (Timoshenko and Woinowsky-Krieger, 1959; Ventsel and Krauthammer, 2002).

Applied to laccoliths, these conditions translate to: (1) the depth ($H$) of the intrusion is small with respect to its diameter ($D$) ($H/D < 0.1$) and (2) the thickness of the intrusion ($T$) is small with respect to its depth ($T/H < 0.2$). The combination of these two conditions implies that the thickness of the intrusion should be much thinner than its diameter ($T/D < 0.02$). Even though models can technically implement thicker and deeper laccoliths (e.g., Scaillet et al., 1995; Bunger and Cruden, 2011), the resulting deformation in the overburden would not respect the models' assumptions, questioning the physical interpretation of these results.

The geometrical characteristics of the Pampa Amarilla laccolith ($H/D = 1.3$ and $T/D = 0.13$) do not fulfill the physical assumptions of the laccolith models based on the thin, stiff elastic plate approximation.

This mismatch between the models' assumptions and these geometrical characteristics is in good agreement with our observations that the growth of the laccolith is controlled dominantly by faulting of the intrusion's overburden. The data of Fig. 12 (Cruden et al., 2018) show that numerous laccoliths on Earth share similar geometric characteristics as that of the Pampa Amarilla laccolith. For most laccoliths included in Fig. 12, the deformation of their overburden is poorly constrained (Corry, 1988, and references therein). The Pampa Amarilla case study suggests that the growth of thick laccoliths may commonly be controlled by faulting of their overburden.

The difference between the end member models based on elastic bending and those based on faulting of the overburden implies distinct scenarios for laccolith growth. The elastic bending model implies that the thickening of the intrusion only happens if the intrusion keeps spreading (Fig. 13, left) (Murdoch, 2002; Bunger and Cruden, 2011; Galland and Scheibert, 2013; Currier and Marsh, 2015; Kavanagh et al., 2015; Scheibert et al., 2017; Kavanagh et al., 2018), even when cooling effects can temporarily halt the lateral spreading (Currier and Marsh, 2015; Thorey and Michaut, 2016). Conversely, in models based on faulting of the overburden, an initial sill thickens and spreads horizontally until reaching a critical diameter, at which point the overburden fails (Fig. 13, right) (Haug et al., 2017; Schmiedel et al., 2017a; Haug et al., 2018; Schmiedel et al., 2019). Subsequently, the intrusion ceases to spread horizontally, and the magma influx is only accommodated by vertical thickening (Fig. 13, right).

The Pampa Amarilla laccolith was emplaced near the bottom of the Vaca Muerta Fm., which is an organic-rich shale formation. Several studies show that the emplacement of igneous intrusions into shale formations in the Neuquén Basin (Vaca Muerta F., Agrio Fm.) is accommodated by shear failure and ductile flow of the host shale (Spacapan et al., 2017; Galland et al., 2019; Magee et al., 2019). These studies show that the tips of sheet-shaped sills propagate by pushing the host rock like an indenter, in disagreement with the main models of sill emplacement based on Linear Elastic Fracture Mechanics (Pollard, 1973; Rubin, 1993). Such a mechanism dominated by inelastic deformation was likely at work during the early phase of emplacement of a sill before the overburden failed and the laccolith thickened. As demonstrated by Román-Berdiel et al. (1995), the emplacement of magma in weak, ductile host formations can greatly control the development of laccoliths.

Note that our study only investigates the structure of the dome induced by the Pampa Amarilla laccolith, which is not exposed. We therefore cannot investigate whether the Pampa Amarilla laccolith formed as a result of emplacement of a single magma pulse or several, successive magma injections, as documented at several laccoliths (de Saint-Blanquat et al., 2006; Leuthold et al., 2012; Wilson et al., 2016; Morgan, 2018; Ruggles et al., 2021). The borehole data from well PA.x-2 shows that above the main andesitic body, a few thin sills were crossed by the well. This suggests that the Pampa Amarilla laccolith might have been emplaced as a result of several successive injections of magma. The number, duration, timing, and volume of each magma pulse cannot be determined.

### 7.2. Internal deformation of the dome

Even though the main faulting occurs along the western peripheral fault of the Pampa Amarilla dome, structural mapping shows that minor faulting also affects the central part of the dome (Figs. 6 and 7). Most evident is an E-W striking normal fault that is subparallel to the long axis of the dome. The distribution of such minor faults is consistent with crestal graben structures occurring above thick shallow intrusions (van Wyk de Vries et al., 2014, and references therein). Similar minor structures associated with magma-induced doming are systematically observed in laboratory models of dome resurgence (Acocella et al., 2001; Acocella and Mulugeta, 2002), laccolith emplacement (Román-Berdiel et al., 1995; Schmiedel et al., 2017a; Schmiedel et al., 2019) and even sill emplacement (Galland, 2012; Schmiedel et al., 2017a). These structures show that outer-arc stretching due to bending occurred in the central parts of the dome, even though the uplift was accommodated by the western boundary fault.

These minor faults show that the structure of the Pampa Amarilla dome is not simple. However, characterization of the detailed structure of the dome would require much better exposure conditions in the central part of the dome, which is hidden by Quaternary deposits. An indirect method for reconstructing the structure of the dome would be through balanced cross sections. However, the main methods for restoring balanced cross sections have been applied to tectonic structures such as rifts and fold-and-thrust belts (Giambiagi et al., 2012; Mescua and Giambiagi, 2012; Lopez-Mir, 2019), where (1) the structures are triggered by horizontal tectonic movements and (2) the structures are dominantly cylindrical and so 2-dimensional profiles perpendicular to the strike of the structures are good approximations. A dome induced by a laccolith is very different: the structure is accommodated by vertical movements of crustal blocks, and the dome is concentric, such that the third dimension becomes an issue for the reconstruction and cylindrical deformation, i.e. perpendicular to the radial profiles, is likely to occur.
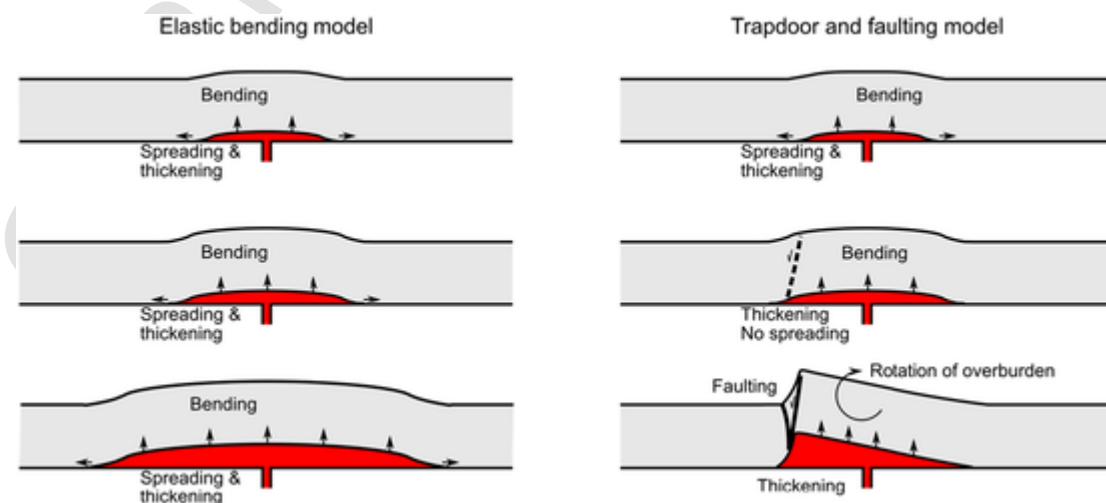


**Fig. 13.** Schematic drawing comparing evolutions of models of laccolith emplacement: model based on elastic bending of the overburden (Pollard and Johnson, 1973; left; from Bunger and Cruden, 2011) versus trapdoor model with faulting of the overburden (right).

### 7.3. Integrated surface and subsurface data

Determining the structure of the Pampa Amarilla laccolith and dome would have not been possible using the subsurface data or the surface geological mapping alone. For example, even if a structure is noticeable on the seismic data, the seismic signal is incoherent (Fig. 4), so that neither the dome nor the intrusion are imaged. In general, our study highlights the need for caution when interpreting seismic data of igneous intrusions (Schofield et al., 2015; Rabbel et al., 2018), even if high-quality data locally reveals complex structures (Bischoff et al., 2020; Reynolds et al., 2021). On the other hand, even though surface geological mapping at Pampa Amarilla indicates the extent of the dome and its trapdoor characteristics, it was necessary to integrate these observations with borehole and seismic data to quantify the amplitude of the dome, and so the thickness of the underlying intrusion. Our study highlights the added value of integrating geological and geophysical data for reconstruction of large igneous intrusions and their associated structures.

### 8. Conclusions

We have described a detailed 3-dimensional structural reconstruction of the Pampa Amarilla dome and the associated subsurface Pampa Amarilla laccolithic intrusion. Our study integrates surface geological observations with subsurface 3D seismic and well data. The conclusions of our study are:

- The Pampa Amarilla dome formed due to the emplacement of a thick subsurface laccolithic intrusion.
- Structural cross sections across the dome were used to estimate that the maximum amplitude of the dome and maximum thickness of the laccolith is ~400 m.
- The dome exhibits a trapdoor structure, with faulting along the western, northwestern and southerwestern edges, and gentle tilting of the overburden to the east. The trapdoor tilting of the laccolith's overburden was the main mechanism that controlled the thickening of the laccolith.
- Minor faulting in the centre of the dome is attributed to 3D stretching of the overburden.
- The reconstructed subsurface Pampa Amarilla laccolith is elliptical in map view, with a 3 km-long E-W axis and a 2 km-long N-S axis. Along E-W cross section, the laccolith is wedge shaped with maximum thickness near its western edge, and exhibits gradual thinning toward the east.
- The emplacement of the relatively thick Pampa Amarilla laccolith, with a thickness-to-length ratio $T/D \sim 0.13$, was mostly accommodated by faulting of the overburden units.
- Given that numerous laccolithic intrusions exhibit similar values of $T/D$, our study suggests that the established mechanical models of laccolith emplacement based on elastic bending of the overburden applies only to few, thin laccoliths/thick sills.

Finally, our study highlights the necessity and value of integrating field geological measurements with subsurface 3D seismic and borehole data for structural reconstructions of subsurface laccolith intrusions.

### Credit author statement

Galland conducted the fieldwork and wrote most of the manuscript.
de la Cal did the fieldwork with Galland, provided the seismic and well data, and edited the manuscript.
Mescua participated to the structural interpretation of the field observations and edited the manuscript.
Rabbel interpreted some seismic data and edited the manuscript.

### Declaration of Competing Interest

The authors declare that they have no known competing financial interests or personal relationships that could have appeared to influence the work reported in this paper.

### Acknowledgements

### References

Acocella, V., Mulugeta, G., 2002. Experiments simulating surface deformation induced by pluton emplacement. Tectonophysics 352, 275–293.

Acocella, V., Cifelli, F., Funiciello, R., 2001. The control of overburden thickness on resurgent domes: insights from analogue models. J. Volcanol. Geotherm. Res. 111, 137–153.

Alsop, G.I., Brown, J.P., Davison, I., Gibling, M.R., 2000. The geometry of drag zones adjacent to salt diapirs. J. Geol. Soc. 157, 1019–1029. https://doi.org/10.1144/jgs.157.5.1019.

Amelung, F., Jonsson, S., Zebker, H., Segall, P., 2000. Widespread uplift and "trapdoor" faulting on Galápagos volcanoes observed with radar interferometry. Nature 407, 993–996. https://doi.org/10.1038/35039604.

Baldauf, P., Stephens, G., Nullo, F.E., Combina, A.M., Kunk, M., 1997. Tertiary Uplift, Magmatism and Sedimentation of the Andes, Southern Mendoza Province, Argentina, Geological Society of America, Abstracts with Program.

Barrionuevo, M., Giambiagi, L., Mescua, J., Suriano, J., de la Cal, H., Soto, J.L., Lossada, A.C., 2019. Miocene deformation in the orogenic front of the Malargüe fold-and-thrust belt (35°30'–36° S): Controls on the migration of magmatic and hydrocarbon fluids. Tectonophysics. https://doi.org/10.1016/j.tecto.2019.06.005.

Bermúdez, A., Delpino, D., 1989. La provincia basáltica andino cuyana. Rev. Asoc. Geol. Argent. 44, 35–55.

Bischoff, A.P., Barrier, A., Beggs, M., Nicol, A., Cole, J.W., 2020. Volcanoes Buried in Te Riu-a-Māui/Zealandia Sedimentary Basins. New Zealand Journal of Geology and Geophysics - IAVCEI Special. Cenozoic Volcanism in New Zealand, Issue. https://doi.org/10.1080/00288306.2020.1773510.

Bunger, A.P., Cruden, A.R., 2011. Modeling the growth of laccoliths and large mafic sills: Role of magma body forces. J. Geophys. Res. 116, B02203. https://doi.org/10.1029/2010jb007648.

Burchardt, S., 2018. Volcanic and Igneous Plumbing Systems - Understanding Magma Transport, Storage, and Evolution in the Earth's Crust. Elsevier, p. 356.

Burchardt, S., Galland, O., 2016. Studying volcanic plumbing systems – Multidisciplinary approaches to a multifaceted problem. In: Nemeth, K. (Ed.), Updates in Volcanology - From Volcano Modelling to Volcano Geology. InTech, pp. 23–53.

Burchardt, S., Mattsson, T., Palma, J.O., Galland, O., Almqvist, B., Mair, K., Jerram, D.A., Hammer, Ø., Sun, Y., 2019. Progressive growth of the Cerro Bayo Cryptodome, Chachahuén Volcano, Argentina—Implications for Viscous Magma Emplacement. J. Geophys. Res. 124, 7934–7961. https://doi.org/10.1029/2019JB017543.

Castro, J.M., Cordonnier, B., Schipper, C.I., Tuffen, H., Baumann, T.S., Feisel, Y., 2016. Rapid laccolith intrusion driven by explosive volcanic eruption. Nat. Commun. 7, 13585. https://doi.org/10.1038/ncomms13585.

Cobbold, P.R., Rossello, E.A., 2003. Aptian to recent compressional deformation, foothills of Neuquén Basin, Argentina. Mar. Pet. Geol. 20, 429–443.

Combina, A.M., Nullo, F., 2011. Ciclos tectónicos, volcánicos y sedimentarios del Cenozoico del sur de Mendoza-Argentina (35°-37°S y 69°30'W). Andean Geol. 38, 198–218.

Corry, C.E., 1988. Laccoliths; Mechanisms of Emplacement and Growth.

Cruden, A.R., McCaffrey, K.J.W., Bunger, A.P., 2018. Geometric scaling of tabular igneous intrusions: implications for emplacement and growth. In: Breitkreuz, C., Rocchi, S. (Eds.), Physical Geology of Shallow Magmatic Systems: Dykes, Sills and Laccoliths. Springer International Publishing, Cham, pp. 11–38.

Currier, R.M., Marsh, B.D., 2015. Mapping real time growth of experimental laccoliths: the effect of solidification on the mechanics of magmatic intrusion. J. Volcanol. Geotherm. Res. 302, 211–224. https://doi.org/10.1016/j.jvolgeores.2015.07.009.

de Saint-Blanquat, M., Habert, G., Horsman, E., Morgan, S.S., Tikoff, B., Launeau, P., Gleizes, G., 2006. Mechanisms and duration of non-tectonically assisted magma emplacement in the upper crust: the Black Mesa pluton, Henry Mountains, Utah. Tectonophysics 428, 1–31. https://doi.org/10.1016/j.tecto.2006.07.014.

Delpino, D., Bermúdez, A., Vitulli, N., Loscerbo, C., 2014. Sistema de petróleo no convencional relacionado con lacolitos eocenos de intraplaca. Área Altiplanicie del Payún, Cuenca Neuquina. In: IX Congreso de Exploración y Desarrollo de Hidrocarburos, Book Sistema de Petróleo no Convencional Relacionado con Lacolitos Eocenos de Intraplaca. Área Altiplanicie del Payún, Cuenca Neuquina, Edition ed. Argentinean Oil and Gas Institute (IAPG). pp. 223–242.

Donnadieu, F., Merle, O., 2001. Geometrical constraints of the 1980 Mount St. Helens intrusion from analogue models. Geophys. Res. Lett. 28, 639–642. https://doi.org/10.1029/2000gl011869.

Fennell, L., Borghi, P., Martos, F., Rosselot, E.A., Naipauer, M., Folguera, A., 2020. The

late cretaceous orogenic system: Early inversion of the Neuquén Basin and Associated Synorogenic Deposits (35˚–38˚ S). In: Kietzmann, D.A., Folguera, A. (Eds.), Opening and Closure of the Neuquén Basin in the Southern Andes. Springer International Publishing, Cham, pp. 303–322.

Galerne, C.Y., Galland, O., Neumann, E.R., Planke, S., 2011. 3D relationships between sills and their feeders: evidence from the Golden Valley Sill complex (Karoo Basin) and experimental modelling. J. Volcanol. Geotherm. Res. 202, 189–199. https://doi.org/10.1016/j.jvolgeores.2011.02.006.

Galland, O., 2012. Experimental modelling of ground deformation associated with shallow magma intrusions. Earth Planet. Sci. Lett. 317–318, 145–156. https://doi.org/10.1016/j.epsl.2011.10.017.

Galland, O., Scheibert, J., 2013. Analytical model of surface uplift above axisymmetric flat-lying magma intrusions: Implications for sill emplacement and geodesy. J. Volcanol. Geotherm. Res. 253, 114–130. https://doi.org/10.1016/j.jvolgeores.2012.12.006.

Galland, O., Hallot, E., Cobbold, P.R., Ruffet, G., de Bremond d'Ars, J., 2007. Volcanism in a compressional Andean setting: a structural and geochronological study of Tromen volcano (Neuquén province, Argentina). Tectonics 26, TC4010. https://doi.org/10.1029/2006TC002011.

Galland, O., Bertelsen, H.S., Eide, C.H., Guldstrand, F., Haug, Ø.T., Leanza, H.A., Mair, K., Palma, O., Planke, S., Rabbel, O., Rogers, B.D., Schmiedel, T., Souche, A., Spacapan, J.B., 2018. Storage and transport of magma in the layered crust-Formation of sills and related flat-lying intrusions. In: Burchardt, S. (Ed.), Volcanic and Igneous Plumbing Systems. Elsevier, pp. 111–136.

Galland, O., Spacapan, J.B., Rabbel, O., Mair, K., Soto, F.G., Eiken, T., Schiuma, M., Leanza, H.A., 2019. Structure, emplacement mechanism and magma-flow significance of igneous fingers – Implications for sill emplacement in sedimentary basins. J. Struct. Geol. 124, 120–135. https://doi.org/10.1016/j.jsg.2019.04.013.

Giambiagi, L., Bechis, F., García, V., Clark, A.H., 2008. Temporal and spatial relationships of thick- and thin-skinned deformation: a case study from the Malargüe fold-and-thrust belt, southern Central Andes. Tectonophysics 459, 123–139. https://doi.org/10.1016/j.tecto.2007.11.069.

Giambiagi, L.B., Ghiglione, M., Cristallini, E., Bottesi, G., 2009. Kinematic models of basement/cover interaction: Insights from the Malargüe fold and thrust belt, Mendoza, Argentina. J. Struct. Geol. 31, 1443–1457. https://doi.org/10.1016/j.jsg.2009.10.006.

Giambiagi, L., Mescua, J., Bechis, F., Tassara, A., Hoke, G.D., 2012. Thrust belts of the southern Central Andes: Along-strike variations in shortening, topography, crustal geometry, and denudation. GSA Bull. 124, 1339–1351. https://doi.org/10.1130/B30609.1.

Gilbert, G.K., 1877. Report on the Geology of the Henry Mountains. U.S. Geogr. Geol. Surv. Rocky Mountain Region (Powel). p. 160.

Groeber, P., 1946. Observaciones geológicas a lo largo del meridiano 70° 1. Hoja Chos Malal. Revista de la Sociedad Geológica Argentina 1, 177–208.

Hansen, D.M., Cartwright, J.A., 2006. The three-dimensional geometry and growth of forced folds above saucer-shaped igneous sills. J. Struct. Geol. 28, 1520–1535.

Haug, Ø.T., Galland, O., Souloumiac, P., Souche, A., Guldstrand, F., Schmiedel, T., 2017. Inelastic damage as a mechanical precursor for the emplacement of saucer-shaped intrusions. Geology 45, 1099–1102. https://doi.org/10.1130/G39361.1.

Haug, Ø.T., Galland, O., Souloumiac, P., Souche, A., Guldstrand, F., Schmiedel, T., Maillot, B., 2018. Shear versus tensile failure mechanisms induced by sill intrusions -- Implications for emplacement of conical and saucer-shaped intrusions. J. Geophys. Res. 123, 3430–3449. https://doi.org/10.1002/2017JB015196.

Hawkes, L., Hawkes, H.K., 1933. The sandfell laccolith and 'dome of elevation'. Q. J. Geol. Soc. 89, 379–398. NP-NP,399–400. https://doi.org/10.1144/gsl.jgs.1933.089.01-04.14.

Hogan, J.P., Price, J.D., Gilbert, M.C., 1998. Magma traps and driving pressure: consequences for pluton shape and emplacement in an extensional regime. J. Struct. Geol. 20, 1155–1168.

Horton, B.K., Fuentes, F., Boll, A., Starck, D., Ramirez, S.G., Stockli, D.F., 2016. Andean stratigraphic record of the transition from backarc extension to orogenic shortening: a case study from the northern Neuquén Basin, Argentina. J. S. Am. Earth Sci. 71, 17–40. https://doi.org/10.1016/j.jsames.2016.06.003.

Howell, J.A., Schwartz, E., Spalletti, L.A., Veiga, G.D., 2005. The Neuquén Basin: an overview. In: Howell, J.A., Schwartz, E., Spalletti, L.A., Veiga, G.D. (Eds.), The Neuquén Basin, Argentina: A Case Study in Sequence Stratigraphy and Basin Dynamics, 252. Geological Society, London, Special Publications, pp. 1–14.

Jackson, M.D., 1997. Processes of laccolithic emplacement in the Southern Henry Mountains, Southeastern Utah. In: Friedman, J.D., Huffman, A.C. (Eds.), Laccolith Complexes of Southeastern Utah: Time of Emplacement and Tectonic Setting - Workshop Proceedings. U.S. Geological Survey Bulletin, 2158, pp. 51–59.

Jackson, M.D., Pollard, D.D., 1990. Flexure and faulting of sedimentary host rocks during growth of igneous domes, Henry Mountains, Utah. J. Struct. Geol. 12, 185–206.

Jackson, C.A.L., Schofield, N., Golenkov, B., 2013. Geometry and controls on the development of igneous sill-related forced-folds: a 2D seismic reflection case study from offshore southern Australia. Geol. Soc. Am. Bull. 125, 1874–1890.

Jaeger, J.C., Cook, N.G.W., Zimmerman, R.W., 2009. Fundamentals of Rock Mechanics. Blackwell Publishing Ltd, Oxford.

Johnson, A.M., Pollard, D.D., 1973. Mechanics of growth of some laccolithic intrusions in the Henry Mountains, Utah, I. Field observations, Gilbert's model, physical properties and flow of the magma. Tectonophysics 18, 261–309.

Jónsson, S., Zebker, H., Amelung, F., 2005. On trapdoor faulting at Sierra Negra volcano, Galápagos. J. Volcanol. Geotherm. Res. 144, 59–71. https://doi.org/10.1016/j.jvolgeores.2004.11.029.

Kavanagh, J.L., Boutelier, D., Cruden, A.R., 2015. The mechanics of sill inception, propagation and growth: Experimental evidence for rapid reduction in magmatic overpressure. Earth Planet. Sci. Lett. 421, 117–128. https://doi.org/10.1016/j.epsl.2015.03.038.

Kavanagh, J.L., Burns, A.J., Hilmi Hazim, S., Wood, E.P., Martin, S.A., Hignett, S., Dennis, D.J.C., 2018. Challenging dyke ascent models using novel laboratory experiments: Implications for reinterpreting evidence of magma ascent and volcanism. J. Volcanol. Geotherm. Res. 354, 87–101. https://doi.org/10.1016/j.jvolgeores.2018.01.002.

Kay, S.M., Burns, W.M., Copeland, P., Mancilla, O., 2006. Upper cretaceous to Holocene magmatism and evidence for transient Miocene shallowing of the Andean subduction zone under the northern Neuquén Basin. Geol. Soc. Am. Spec. Pap. 407, 19–60.

Kennedy, B., Wilcock, J., Stix, J., 2012. Caldera resurgence during magma replenishment and rejuvenation at Valles and Lake City calderas. Bull. Volcanol. 74, 1833–1847. https://doi.org/10.1007/s00445-012-0641-x.

Kerr, A.D., Pollard, D.D., 1998. Toward more realistic formulations for the analysis of laccoliths. J. Struct. Geol. 20, 1783–1793.

Koch, F.G., Johnson, A.M., Pollard, D.D., 1981. Monoclinal bending of strata over laccolithic intrusions. Tectonophysics 74, T21–T31. https://doi.org/10.1016/0040-1951(81)90189-X.

Kraemer, P., Silvestro, J., Achilli, F., Brinkworth, W., 2011. Kinematics of a hybrid thick-thin-skinned fold and thrust belt recorded in neogene syntectonic Wedge-top basins, Southern Central Andes between 35 and 36S, Malargue, Argentina. In: McClay, K., Shaw, J., Suppe, J. (Eds.), Thrust Fault-Related Folding, 94. AAPG, pp. 245–270.

Leuthold, J., Müntener, O., Baumgartner, L.P., Putlitz, B., Ovtcharova, M., Schaltegger, U., 2012. Time resolved construction of a bimodal laccolith (Torres del Paine, Patagonia). Earth Planet. Sci. Lett. 325–326, 85–92. https://doi.org/10.1016/j.epsl.2012.01.032.

Litvak, V.D., Spagnuolo, M.G., Folguera, A., Poma, S., Jones, R.E., Ramos, V.A., 2015. Late Cenozoic calc-alkaline volcanism over the Payenia shallow subduction zone, South-Central Andean back-arc (34˚30'–37˚S), Argentina. J. S. Am. Earth Sci. 64, 365–380. https://doi.org/10.1016/j.jsames.2015.09.010.

Lopez-Mir, B., 2019. Chapter 1 - Cross-section construction and balancing: examples from the Spanish Pyrenees. In: Billi, A., Fagereng, Å. (Eds.), Developments in Structural Geology and Tectonics, vol. 5. Elsevier, pp. 3–23.

Magee, C., Briggs, F., Jackson, C.A.L., 2013. Lithological controls on igneous intrusion-induced ground deformation. J. Geol. Soc. 170, 853–856.

Magee, C., Muirhead, J.D., Karvelas, A., Holford, S.P., Jackson, C.A.L., Bastow, I.D., Schofield, N., Stevenson, C.T.E., McLean, C., McCarthy, W., Shtukert, O., 2016. Lateral magma flow in mafic sill complexes. Geosphere 12, 809–841. https://doi.org/10.1130/ges01256.1.

Magee, C., Bastow, I.D., van Wyk de Vries, B., Jackson, C.A.-L., Hetherington, R., Hagos, M., Hoggett, M., 2017. Structure and dynamics of surface uplift induced by incremental sill emplacement. Geology 45, 431–434. https://doi.org/10.1130/g38839.1.

Magee, C., Muirhead, J.D., Schofield, N., Walker, R.J., Galland, O., Holford, S., Spacapan, J.B., Jackson, C.A.L., McCarthy, W., 2019. Structural signatures of igneous sheet intrusion propagation. J. Struct. Geol. 125, 148–154. https://doi.org/10.1016/j.jsg.2018.07.010.

Manceda, R., Figueroa, D., 1993. La inversión del rift Mesozoico en la faja fallada y plegada de Malargüe. Provincia de Mendoza. In: XII Congreso Geológico Argentina y II Congreso de Exploración de Hidrocarburos, Book La Inversión del rift Mesozoico en la Faja Fallada y Plegada de Malargüe. Provincia de Mendoza, 12, pp. 219–232. Edition ed.

Manceda, R., Figueroa, D., Suarez, S., 1995. Inversion of the Mesozoic Neuquén rift in the Malargüe fold and thrust belt, Mendoza, Argentina. In: Tankard, A.J., Welsink, H.J. (Eds.), Petroleum Basins of South America: AAPG Memoir. pp. 369–382. 62, pp.

Mark, N.J., Schofield, N., Pugliese, S., Watson, D., Holford, S., Muirhead, D., Brown, R., Healy, D., 2018. Igneous intrusions in the Faroe Shetland basin and their implications for hydrocarbon exploration; new insights from well and seismic data. Mar. Pet. Geol. 92, 733–753. https://doi.org/10.1016/j.marpetgeo.2017.12.005.

Mattsson, T., Burchardt, S., Almqvist, B.S.G., Ronchin, E., 2018. Syn-Emplacement Fracturing in the Sandfell Laccolith, Eastern Iceland—Implications for Rhyolite Intrusion Growth and Volcanic Hazards. Frontiers 6. https://doi.org/10.3389/feart.2018.00005.

Mescua, J.F., Giambiagi, L.B., 2012. Fault inversion vs. new thrust generation: a case study in the Malargüe fold-and-thrust belt, Andes of Argentina. J. Struct. Geol. 35, 51–63. https://doi.org/10.1016/j.jsg.2011.11.011.

Mescua, J.F., Giambiagi, L.B., Tassara, A., Gimenez, M., Ramos, V.A., 2014. Influence of pre-Andean history over Cenozoic foreland deformation: Structural styles in the Malargüe fold-and-thrust belt at 35°S, Andes of Argentina. Geosphere 10, 585–609. https://doi.org/10.1130/GES00939.1.

Michaut, C., 2011. Dynamics of magmatic intrusions in the upper crust: Theory and applications to laccoliths on Earth and the Moon. J. Geophys. Res. 116, B05205. https://doi.org/10.1029/2010jb008108.

Michel, J., Baumgartner, L., Putlitz, B., Schaltegger, U., Ovtcharova, M., 2008. Incremental growth of the Patagonian Torres del Paine laccolith over 90 k.y. Geology 36, 459–462. https://doi.org/10.1130/g24546a.1.

Minakami, T., Ishikawa, T., Yagi, K., 1951. The 1944 eruption of volcano Usu in Hokkaido, Japan. Volcanol. Bull. Ser. 2 (11), 5–157.

Morgan, S.S., 2018. Chapter 6 - Pascal's Principle, a simple Model to Explain the Emplacement of Laccoliths and some Mid-crustal Plutons. In: Burchardt, S. (Ed.), Volcanic and Igneous Plumbing Systems. Elsevier, pp. 139–165.

Murdoch, L.C., 2002. Mechanical analysis of idealized shallow hydraulic fracture. J. Geotech. Geoenviron. Eng. 128. https://doi.org/10.1061/(ASCE)1090-0241(2002)128:6(488).

Nullo, F.E., Stephens, G.C., Otamendi, J., Baldauf, P.E., 2002. El volcanismo del Tertiario superior del sur de Mendoza. Rev. Asoc. Geol. Argent. 57, 119–132.

Pollard, D.D., 1973. Derivation and evaluation of a mechanical model for sheet intrusions.

Tectonophysics 19, 233–269. https://doi.org/10.1016/0040-1951(73)90021-8.

Pollard, D.D., Johnson, A.M., 1973. Mechanics of growth of some laccolithic intrusions in the Henry Mountains, Utah, II. Bending and failure of overburden layers and sill formation. Tectonophysics 18, 311–354.

Rabbel, O., Galland, O., Mair, K., Lecomte, I., Senger, K., Spacapan, J.B., Manceda, R., 2018. From field analogues to realistic seismic modelling: a case study of an oil-producing andesitic sill complex in the Neuquén Basin, Argentina. J. Geol. Soc. https://doi.org/10.1144/jgs2017-116.

Ramos, V.A., Folguera, A., 2011. Payenia volcanic province in the Southern Andes: an appraisal of an exceptional Quaternary tectonic setting. J. Volcanol. Geotherm. Res. 201, 53–64. https://doi.org/10.1016/j.jvolgeores.2010.09.008.

Renard, F., McBeck, J., Kandula, N., Cordonnier, B., Meakin, P., Ben-Zion, Y., 2019. Volumetric and shear processes in crystalline rock approaching faulting. Proc. Natl. Acad. Sci. 116, 16234. https://doi.org/10.1073/pnas.1902994116.

Reynolds, P., Holford, S., Schofield, N., Ross, A., 2021. 3D seismic reflection constraints on the emplacement of mafic laccoliths and their role in shallow crustal magma transport: a case study from the ceduna sub-basin, Great Australian Bight. Mar. Pet. Geol. 105419. https://doi.org/10.1016/j.marpetgeo.2021.105419.

Rocchi, S., Westerman, D.S., Dini, A., Innocenti, F., Tonarini, S., 2002. Two-stage growth of laccoliths at Elba Island, Italy. Geology 30, 983–986. https://doi.org/10.1130/0091-7613(2002)030<0983:tsgola>2.0.co;2.

Rocchi, S., Dini, A., Mazzarini, F., Westerman, D.S., 2010. Introduction: LASI III - Magma pulses and sheets in tabular intrusions. Geosphere 6, 161–162.

Rodriguez Monreal, F., Villar, H.J., Baudino, R., Delpino, D., Zencich, S., 2009. Modeling an atypical petroleum system: a case study of hydrocarbon generation, migration and accumulation related to igneous intrusions in the Neuquén Basin, Argentina. Mar. Pet. Geol. 26, 590–605. https://doi.org/10.1016/j.marpetgeo.2009.01.005.

Román-Berdiel, T., Gapais, D., Brun, J.P., 1995. Analogue models of laccolith formation. J. Struct. Geol. 17, 1337–1346.

Rubin, A.M., 1993. Tensile fracture of rock at high confining pressure: Implications for dike propagation. J. Geophys. Res. 98, 15919–15935. https://doi.org/10.1029/93jb01391.

Rubin, A.M., 1995. Propagation of magma-filled cracks. Annu. Rev. Earth Planet. Sci. 23, 287–336.

Ruggles, C.E., Morgan, S.S., Reber, J.E., 2021. A multiple-pulse emplacement model for the Shonkin Sag laccolith, Montana, USA. J. Struct. Geol. 149, 104378. https://doi.org/10.1016/j.jsg.2021.104378.

Scaillet, B., Pêcher, A., Rochette, P., Champenois, M., 1995. The Gangotri granite (Garhwal Himalaya): Laccolithic emplacement in an extending collisional belt. J. Geophys. Res. 100, 585–607.

Scheibert, J., Galland, O., Hafver, A., 2017. Inelastic deformation during sill and laccolith emplacement: insights from an analytic elasto-plastic model. J. Geophys. Res. 122, 923–945. https://doi.org/10.1002/2016JB013754.

Schiuma, M.F., 1994. Intrusivos del valle del Río Grande, Provincia de Mendoza, su Importancia Como Productores de Hidrocarburos, Facultad de Ciencias Naturales y Museo. Universidad Nacional de La Plata, La Plata.

Schiuma, M., Llambías, E.J., 2014. Importancia de los sills como reservorios en la Cuenca Neuquina del sur de Mendoza. In: IX Congreso de Exploración y Desarrollo de Hidrocarburos, Book Importancia de los sills como reservorios en la Cuenca Neuquina del sur de Mendoza, Edition ed., IAPG, Trabajos Técnicos I, pp. 331–349.

Schmiedel, T., Galland, O., Breitkreuz, C., 2017a. Dynamics of sill and laccolith emplacement in the brittle crust: role of host rock strength and deformation mode. J. Geophys. Res. 122, 8625–9484. https://doi.org/10.1002/2017JB014468.

Schmiedel, T., Kjoberg, S., Planke, S., Magee, C., Galland, O., Schofield, N., Jackson, C.A.-L., Jerram, D.A., 2017b. Mechanisms of overburden deformation associated with the emplacement of the Tulipan sill, mid-Norwegian margin. Interpretation 5, SK23-SK38. https://doi.org/10.1190/int-2016-0155.1.

Schmiedel, T., Galland, O., Haug, Ø.T., Dumazer, G., Breitkreuz, C., 2019. Coulomb failure of Earth's brittle crust controls growth, emplacement and shapes of igneous sills, saucer-shaped sills and laccoliths. Earth Planet. Sci. Lett. 510, 161–172. https://doi.org/10.1016/j.epsl.2019.01.011.

Schofield, N., Holford, S.P., Millett, J., Brown, D.J., Jolley, D., Passey, S.R., Muirhead, D., Grove, C., Magee, C., Murray, J., Hole, M., Jackson, C.A.L., Stevenson, C.T., 2015. Regional magma plumbing and emplacement mechanisms of the Faroe-Shetland Sill complex: implications for magma transport and petroleum systems within sedimentary basins. Basin Res. https://doi.org/10.1111/bre.12164.

Sigmarsson, O., Vlastelic, I., Andreasen, R., Bindeman, I., Devidal, J.L., Moune, S., Keiding, J.K., Larsen, G., Höskuldsson, A., Thordarson, T., 2011. Remobilization of silicic intrusion by mafic magmas during the 2010 Eyjafjallajökull eruption. Solid Earth 2, 271–281. https://doi.org/10.5194/se-2-271-2011.

Søager, N., Holm, P.M., Llambías, E.J., 2013. Payenia volcanic province, southern Mendoza, Argentina: OIB mantle upwelling in a backarc environment. Chem. Geol. 349–350, 36–53. https://doi.org/10.1016/j.chemgeo.2013.04.007.

Spacapan, J.B., Galland, O., Leanza, H.A., Planke, S., 2016. Control of strike-slip fault on dyke emplacement and morphology. J. Geol. Soc. 173, 573–576. https://doi.org/10.1144/jgs2015-166.

Spacapan, J.B., Galland, O., Leanza, H.A., Planke, S., 2017. Igneous sill and finger emplacement mechanism in shale-dominated formations: a field study at Cuesta del Chihuido, Neuquén Basin, Argentina. J. Geol. Soc. 174, 422–433. https://doi.org/10.1144/jgs2016-056.

Spacapan, J., Palma, J., Galland, O., Manceda, R., Rocha, E., D'Odorico, A., Leanza, H., 2018a. Thermal impact of igneous sill-complexes on organic-rich formations and implications for petroleum systems: a case study in the northern Neuquén Basin, Argentina. Mar. Pet. Geol. 91, 519–531.

Spacapan, J.B., Palma, O., Galland, O., Manceda, R., Rocha, E., D'Odorico, A., Leanza, H.A., 2018b. Thermal impact of igneous sill complexes on organic-rich formations and the generation of a petroleum system: case study in the Neuquén Basin, Argentina. Mar. Pet. Geol. 91, 519–531. https://doi.org/10.1016/j.marpetgeo.2018.01.018.

Spacapan, J.B., D'Odorico, A., Palma, O., Galland, O., Rojas Vera, E., Ruiz, R., Leanza, H.A., Medialdea, A., Manceda, R., 2020. Igneous petroleum systems in the Malargüe fold and thrust belt, Río Grande Valley area, Neuquén Basin, Argentina. Mar. Pet. Geol. 111, 309–331. https://doi.org/10.1016/j.marpetgeo.2019.08.038.

Stevenson, C.T.E., Owens, W.H., Hutton, D.H.W., Hood, D.N., Meighan, I.G., 2007. Laccolithic, as opposed to cauldron subsidence, emplacement of the Eastern Mourne pluton, N. Ireland: evidence from anisotropy of magnetic susceptibility. J. Geol. Soc. 164, 99. https://doi.org/10.1144/0016076492006-008.

Thorey, C., Michaut, C., 2014. A model for the dynamics of crater-centered intrusion: Application to lunar floor-fractured craters. J. Geophys. Res. Planets 119, 286–312. https://doi.org/10.1002/2013JE004467.

Thorey, C., Michaut, C., 2016. Elastic-plated gravity currents with a temperature-dependent viscosity. J. Fluid Mech. 805, 88–117. https://doi.org/10.1017/jfm.2016.538.

Timoshenko, S., Woinowsky-Krieger, S., 1959. Theory of Plates and Shells. McGraw-Hill Book Company, New York.

Trude, J., Cartwright, J., Davies, R.J., Smallwood, J., 2003. New technique for dating igneous sills. Geology 31, 813–816.

Valencio, D.A., Linares, E., Creer, K.M., 1970. Paleomagnetismo y Edades Geológicas de Algunos Basaltos Terciarios y Cuartarios de Mendoza y Neuquén. Actas 4tas. Jornadas Geológicas Argentinas. pp. 397–415.

van Wyk de Vries, B., Márquez, A., Herrera, R., Bruña, J.L.G., Llanes, P., Delcamp, A., 2014. Craters of elevation revisited: forced-folds, bulging and uplift of volcanoes. Bull. Volcanol. 76, 875. https://doi.org/10.1007/s00445-014-0875-x.

Veiga, R.D., Vergani, G.D., Brissón, I.E., Macellari, C.E., Leanza, H.A., 2020. The Neuquén super basin. AAPG Bull. 104, 2521–2555. https://doi.org/10.1306/09092020023.

Ventsel, E., Krauthammer, T., 2002. Thin plates and shells: Theory, analysis, and applications. Appl. Mech. Rev. 55, B72–B73. https://doi.org/10.1115/1.1483356.

Vergani, G.D., Tankard, A.J., Belotti, H.J., Welsink, H.J., 1995. Tectonic evolution and paleogeography of the Neuquén basin, Argentina. In: Tankard, A.J., Suárez, R., Welsink, H.J. (Eds.), Petroleum Basins of South America. American Association of Petroleum Geology Memoir, 62, pp. 383–402.

Westerman, D.S., Rocchi, S., Breitkreuz, C., Stevenson, C.T., Wilson, P.I.R., 2018. Structures related to the emplacement of shallow-level intrusions. In: Breitkreuz, C., Rocchi, S. (Eds.), Physical Geology of Shallow Magmatic Systems: Dykes, Sills and Laccoliths. Springer International Publishing, Cham, pp. 83–118.

Wilson, P.I.R., McCaffrey, K.J.W., Wilson, R.W., Jarvis, I., Holdsworth, R.E., 2016. Deformation structures associated with the Trachyte Mesa intrusion, Henry Mountains, Utah: Implications for sill and laccolith emplacement mechanisms. J. Struct. Geol. 87, 30–46. https://doi.org/10.1016/j.jsg.2016.04.001.

Witkind, I.J., 1973. Igneous Rocks and Related Mineral Deposits of the Barker Quadrangle, Little Belt Mountains, Montana, Professional Paper U. S. Geological Survey. 752. p. 58.

Witte, J., Bonora, M., Carbone, C., Oncken, O., 2012. Fracture evolution in oil-producing sills of the Rio Grande Valley, northern Neuquén Basin, Argentina. AAPG Bull. 96, 1253–1277. https://doi.org/10.1306/10181110152.

Yagupsky, D.L., Cristallini, E.O., Zamora Valcarce, G., Varadé, R., 2007. Sistema compresivo sobreimpuesto a un rift oblicuo: aplicaciones en la faja plegada y corrida de Malargüe, sur de Mendoza. Rev. Asoc. Geol. Argent. 62, 124–138.

Yagupsky, D.L., Cristallini, E.O., Fantín, J., Valcarce, G.Z., Bottesi, G., Varadé, R., 2008. Oblique half-graben inversion of the Mesozoic Neuquén Rift in the Malargüe Fold and Thrust Belt, Mendoza, Argentina: New insights from analogue models. J. Struct. Geol. 30, 839–853. https://doi.org/10.1016/j.jsg.2008.03.007.

YPF, 1976. Unpublished internal report: Plano Geológico Zona Pampa Amarilla-Agua Botada.